



Deposited via The University of Sheffield.

White Rose Research Online URL for this paper:

<https://eprints.whiterose.ac.uk/id/eprint/184693/>

Version: Published Version

Article:

Paris, J.R., Whiting, J.R., Daniel, M.J. et al. (2022) A large and diverse autosomal haplotype is associated with sex-linked colour polymorphism in the guppy. *Nature Communications*, 13 (1). 1233. ISSN: 2041-1723

<https://doi.org/10.1038/s41467-022-28895-4>

Reuse





This article is distributed under the terms of the Creative Commons Attribution (CC BY) licence. This licence allows you to distribute, remix, tweak, and build upon the work, even commercially, as long as you credit the authors for the original work. More information and the full terms of the licence here:

<https://creativecommons.org/licenses/>

Takedown

If you consider content in White Rose Research Online to be in breach of UK law, please notify us by emailing eprints@whiterose.ac.uk including the URL of the record and the reason for the withdrawal request.

A large and diverse autosomal haplotype is associated with sex-linked colour polymorphism in the guppy

Josephine R. Paris ^{1✉}, James R. Whiting¹, Mitchel J. Daniel², Joan Ferrer Obiol ³, Paul J. Parsons ^{1,4}, Mijke J. van der Zee¹, Christopher W. Wheat⁵, Kimberly A. Hughes ² & Bonnie A. Fraser¹

Male colour patterns of the Trinidadian guppy (*Poecilia reticulata*) are typified by extreme variation governed by both natural and sexual selection. Since guppy colour patterns are often inherited faithfully from fathers to sons, it has been hypothesised that many of the colour trait genes must be physically linked to sex determining loci as a ‘supergene’ on the sex chromosome. Here, we phenotype and genotype four guppy ‘Iso-Y lines’, where colour was inherited along the patriline for 40 generations. Using an unbiased phenotyping method, we confirm the breeding design was successful in creating four distinct colour patterns. We find that genetic differentiation among the Iso-Y lines is repeatedly associated with a diverse haplotype on an autosome (LG1), not the sex chromosome (LG12). Moreover, the LG1 haplotype exhibits elevated linkage disequilibrium and evidence of sex-specific diversity in the natural source population. We hypothesise that colour pattern polymorphism is driven by Y-autosome epistasis.

¹Department of Biosciences, University of Exeter, Stocker Road, Exeter EX4 4QD, UK. ²Department of Biological Science, Florida State University, 319 Stadium Drive, Tallahassee, FL 32304, USA. ³Departament de Microbiologia, Genètica i Estadística and Institut de Recerca de la Biodiversitat, Universitat de Barcelona, Barcelona, Catalonia, Spain. ⁴NERC Environmental Omics Facility, School of Biosciences, University of Sheffield, Sheffield S10 2TN, UK. ⁵Department of Zoology, Stockholm University, Stockholm, Sweden. ✉email: j.r.paris@exeter.ac.uk

Understanding the genetic architecture of highly diverse and ecologically-important traits is a fundamental problem in evolutionary biology. This is particularly true for traits where the underlying genes are predicted to be on the Y chromosome. Because the Y-chromosome does not recombine, it is expected to degrade over time, whilst its unique inheritance from fathers to sons will select for genes that increase male fitness¹. However, this model neglects important factors such as pleiotropy and epistasis^{2,3}. Sex-linked colour polymorphism provides a tractable trait for exploring the evolutionary and ecological drivers of balancing selection and sex-chromosome evolution^{4,5}, and genome sequencing methods have hugely enhanced our ability to detect the genetic basis of colour traits⁶. Using a unique breeding strategy designed to delineate regions of the genome related to colour, we analyse whole-genome sequencing data to uncover the genetic basis of sex-linked colour polymorphism in the Trinidadian guppy (*Poecilia reticulata*).

Guppy colour traits have fascinated biologists for a hundred years, and present an exciting system for testing predictions of sex-linked polymorphic traits. Males display a mosaic of complex and diverse colouration patterns, varying in colour, number, shape, size, and position of spots, while females are a drab and uniform tan colour^{7,8}. Guppy colour patterns exhibit high levels of standing genetic variation^{9–11}, despite evidence that mate choice and predation impose directional selection^{12–15}. Considerable evidence suggests that genetic diversity is maintained by negative frequency dependent selection (NFDS), driven by female mate preference for rare or novel morphs^{16–20} and also frequency-dependent survival^{21,22}. Despite this great diversity in colour patterns, and our understanding of the evolutionary processes maintaining it, the underlying genetic architecture remains largely unknown.

It has long-been hypothesised that colour patterning genes and the sex determining locus (SDL) form a Y-linked ‘supergene’ in the guppy^{23,24}. The supergene-hypothesis originates from early pedigree studies that found patrilineal inheritance for many guppy colour pattern elements^{25,26}. While clearly demonstrating the importance of the Y-chromosome for colour, this early work also reported among-population variability in the strength of Y-linkage, indicating a more complex genetic architecture. Indeed, although there is an enrichment of pigment genes on male-specific contigs²⁷, recent studies have also highlighted the importance of X-linked and autosomal inheritance of colour traits. A QTL mapping study found that only 13% of colour trait loci mapped to the sex chromosome (LG12)²⁸ and a pedigree analysis of colour pattern inheritance showed that ornaments are not completely Y-linked, hypothesising a potential role for Y-autosome epistasis²⁹. Combined, this work suggests that a non-recombining, male-specific region on LG12 plays an important, but not exclusive role in guppy colour patterning.

Recent genomic studies have therefore focussed on identifying the boundaries and genetic content of the non-recombining Y-region. Using male specific diversity across multiple populations, the Y-specific region was concluded to be small, possibly only a single gene, occurring near the distal end of LG12^{30–32}. Indeed, sex has been mapped to the distal end of LG12 in multiple mapping and pedigree crossing studies^{28,30,33}. Other studies however, conclude that the non-recombining region extends beyond this distal region in some populations based on similar sex-specific genomic diversity measures^{34,35}. Intriguingly, the distal end of LG12 has been found to be highly diverse among males with many segregating male-specific variants, indicative of multiple Y haplotypes, as would be predicted under NFDS for Y-linked colour traits^{31,35}. Within this candidate region, however, no gene associated with colour or sex has been found. Clearly, more work is needed to delineate the Y-linked genomic architecture of this important trait.

In this work, we use an innovative approach to identify genomic regions associated with highly variable, sex-linked, colour polymorphism in guppies. We phenotype and genotype four ‘Iso-Y’ lines, which originated from a natural population, and show strong Y-linked parental heritability in colour pattern^{19,36}. Each Iso-Y line was founded by one male showing a distinct colour pattern. This colour pattern was introgressed onto a randomised genetic background by mating males that resembled the founder, to females from a randomly-mating stock population. Outcrossing to stock population females occurred every 2–3 generations over the 40 generations that the lines were propagated. Given that each backcrossed generation theoretically reduces the parental genome by half, we expect more than 99.99% of the genome to be homogenised through this approach³⁷. This experimental design allows us to delineate regions of the genome related to colour pattern, as it should homogenise regions unrelated to the colour differences among lines. Using a Pool-seq approach on each Iso-Y line, we find that the lines are consistently different on an autosome (LG1), not the sex chromosome (LG12). In order to examine the LG1 colour-linked candidates in a natural population, we then conduct an analysis of whole-genome sequencing (WGS) data from the source population, finding that a large and diverse autosomal haplotype is maintained in nature. We hypothesise that colour pattern variation is driven by Y-autosome epistasis. This genetic architecture could help to explain how high levels of Y-linked diversity is maintained in guppy colour patterns.

Results

Iso-Y lines are distinct across multiple dimensions of colour.

Male guppies have an ultraviolet component to their colour patterns, and guppies can detect and adjust their social behaviour based on ultraviolet colouration³⁸. Consequently, we used multispectral digital photography to capture human-visible and ultraviolet images of males from each Iso-Y line. We used geometric morphometrics to correct for individual differences in body size and shape among fish so that colour patterns could be measured as though they existed on identical male bodies. We then used the Colormesh pipeline³⁹ to extract colour measurements from these images at sampling locations across the body and caudal fin.

Discriminant analysis of principal components (DAPC)^{40,41} (see ‘Methods’ for details) revealed that males from the different Iso-Y lines were well-separated based on colour pattern. Discriminant functions (DF) 1, 2 and 3 accounted for 51.9%, 36.8%, and 11.4% of the variation among the Iso-Y lines, respectively (Fig. 1a), and distinguished Iso-Y9 from the other Iso-Y lines along axis 1. Axis 2 predominantly separated Iso-Y10, and axis 3 subtly differentiated the lines (Supplementary Fig. 1). Colour variation on the caudal peduncle and in the anal region were most important for differentiating the Iso-Y lines (Fig. 1b). Variation in the red colour channel associated with DF1 captured the orange colour spot observed on the anal region in Iso-Y9 (Fig. 1c).

The Iso-Y lines also showed robust phenotypic differences when we examined mean colour measures using permutational MANOVA. Here, we reduced the dimensionality of the colour pattern data using PCA, with 17 PC’s explaining 59.3% of the total variation in colour measurements (see Supplementary Fig. 2 for PC distributions of each of the Iso-Y lines). The omnibus test indicated significant overall differences among Iso-Y lines ($df = 3169$, pseudo- $F = 23.66$, $P < 0.001$). Post-hoc pairwise tests revealed significant differences in colour pattern among all pairs (all $P < 0.001$; see Supplementary Table 1). Based on centroid distances, the greatest phenotypic differences were between Iso-

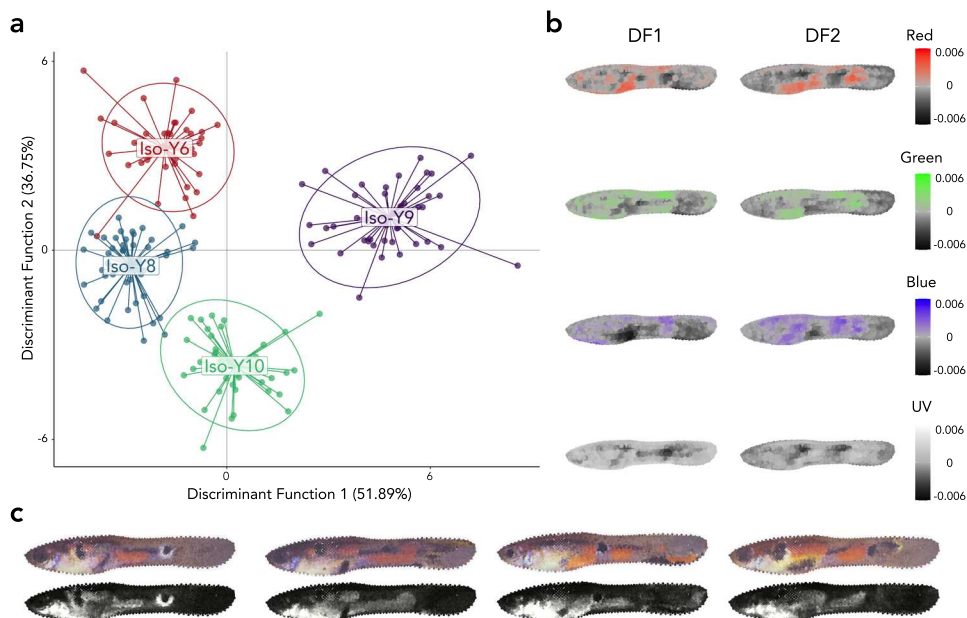


Fig. 1 Discriminant analysis of principal components (DAPC) differentiating colour measurements among Iso-Y lines. **a** Scatterplot of the first 2 Discriminant Functions: Discriminant Function 1 (DF1) and Discriminant Function 2 (DF2). Each point represents a male, and colour denotes the Iso-Y line. **b** Heatmaps for each colour channel depicting the correlation between colour at each sampling location for Discriminant Function 1 (DF1) or Discriminant Function 2 (DF2). **c** Images of the male closest to each Iso-Y line's centroid, constructed from the Red Green Blue (RGB; top) and ultraviolet (UV; bottom) colour measurements at each sampling location. UV images are false colour, with lighter grey indicating higher UV reflectance. Source data underlying Fig. 1a are provided as a Source data file.

Y6 and Iso-Y10 and the smallest phenotypic differences between Iso-Y6 and Iso-Y8. Using permutational t-tests to determine whether the Iso-Y lines differ in phenotypic variance, we found that Iso-Y9 was significantly more variable (Supplementary Table 2; Supplementary Fig. 3).

Iso-Y lines are consistently different on an autosome. Using a pooled whole-genome sequencing (Pool-seq) approach and summarising all pairwise comparisons with a PCA, we were able to identify where along the genome the Iso-Y lines were consistently different (Fig. 2). Pool-seq of each of the four Iso-Y lines ($n_{\text{per line}} = 48$) resulted in a final dataset of 3,995,905 SNPs. Mean pairwise F_{ST} between the Iso-Y lines was high overall ($F_{\text{ST}} = 0.091$). We first used pairwise F_{ST} values among the four Iso-Y lines, and then used a multivariate approach by normalising F_{ST} to $Z\text{-}F_{\text{ST}}$ and summarising these with PCA F_{ST}^{42} . The aim here was to summarise covariance of F_{ST} among comparisons and assess whether certain regions were consistently differentiated among the Iso-Y lines. $Z\text{-}F_{\text{ST}}$ PC1 accounted for 37% of the total variance and reflected positive covariance in all pairwise F_{ST} comparisons (Supplementary Table 3).

LG1 and LG12 showed excess divergence among the Iso-Y lines and were clear outliers compared to the rest of the genome (Fig. 2a). LG1 and LG12 both had the highest chromosome-wide average $Z\text{-}F_{\text{ST}}$ PC1 scores (LG1 = 1.48; LG12 = 1.62) and the highest percentage of SNPs with a $Z\text{-}F_{\text{ST}}$ PC1 score above an upper 95% quantile of 3 (LG1 = 24%; LG12 = 29%). The remaining 47% of high-scoring SNPs were distributed across the genome, with other individual chromosomes or scaffolds accounting for <7% of high-scoring SNPs (according to an upper 95% quantile of 3; Supplementary Fig. 4). Other chromosomes showed inconsistent regions of localised differentiation (Supplementary Fig. 5) and we found no evidence indicative of a genome-wide relationship between recombination and $Z\text{-}F_{\text{ST}}$ PC1 (Supplementary Fig. 6). Thus, LG1 and LG12 became our focus for investigating differentiation among the Iso-Y lines.

Interestingly, the patterns of differentiation were different for these two focal chromosomes. $Z\text{-}F_{\text{ST}}$ PC1 indicated three regions of high differentiation on LG1 (Fig. 2b). On LG12, these scores were elevated consistently along the entire chromosome (Fig. 2d).

By performing an additional PCA on LG1, we found good agreement between the areas of differentiation amongst the Iso-Y lines. $Z\text{-}F_{\text{ST}}\text{-}LG1$ PC1 (52% of the total variance) showed high positive loadings among five of the six pairwise comparisons (Iso-Y6–Iso-Y8 being the exception; Supplementary Table 4), which was also reflected in the per-SNP pairwise F_{ST} comparisons, where Iso-Y6 and Iso-Y8 exhibited the lowest differentiation (Supplementary Fig. 7; Supplementary Table 5). The Iso-Y6–Iso-Y8 comparison loaded positively onto PC2 (17% of total variance) and $Z\text{-}F_{\text{ST}}$ PC2 (and to some extent, PC3) highlighted the same regions of differentiation as PC1 (Supplementary Fig. 8). We found no relationship between $Z\text{-}F_{\text{ST}}$ PC1 scores and the recombination landscape on LG1 (Supplementary Fig. 9).

In contrast, PC axis loadings for $Z\text{-}F_{\text{ST}}$ on LG12 were different among the Iso-Y lines (Supplementary Table 6). This was also apparent in per-SNP pairwise F_{ST} values (Supplementary Fig. 10). All comparisons with Iso-Y9 loaded strongly onto PC1 (PC1 captured 37% of the total variance), suggesting Iso-Y9 is the most differentiated line on LG12. This was consistent with pairwise F_{ST} , where Iso-Y9 had the highest mean pairwise F_{ST} SNPs (>0.2) and thus high $Z\text{-}F_{\text{ST}}\text{-}LG12$ PC1 scores reflected the haplotype associated with the Iso-Y9 phenotype. $Z\text{-}F_{\text{ST}}\text{-}LG12$ PC2 (PC2 captured 30% of total variance) loadings were high for the remaining two comparisons with Iso-Y6. This suggests SNPs with high $Z\text{-}F_{\text{ST}}\text{-}LG12$ PC2 scores reflect the haplotype associated with the Iso-Y6 phenotype. $Z\text{-}F_{\text{ST}}\text{-}LG12$ PC3 reflected the final comparison, Iso-Y8–Iso-Y10. $Z\text{-}F_{\text{ST}}\text{-}LG12$ PC2 and PC3 also reflected Iso-Y line-specific loadings (Supplementary Fig. 11). Taken together, this demonstrates that Iso-Y specific haplotypes co-occur at the same regions on LG1, whereas on LG12, the Iso-Y specific haplotypes occur in different regions.

We were able to further identify areas of consistent divergence in three regions on LG1 using change point detection (CPD) on

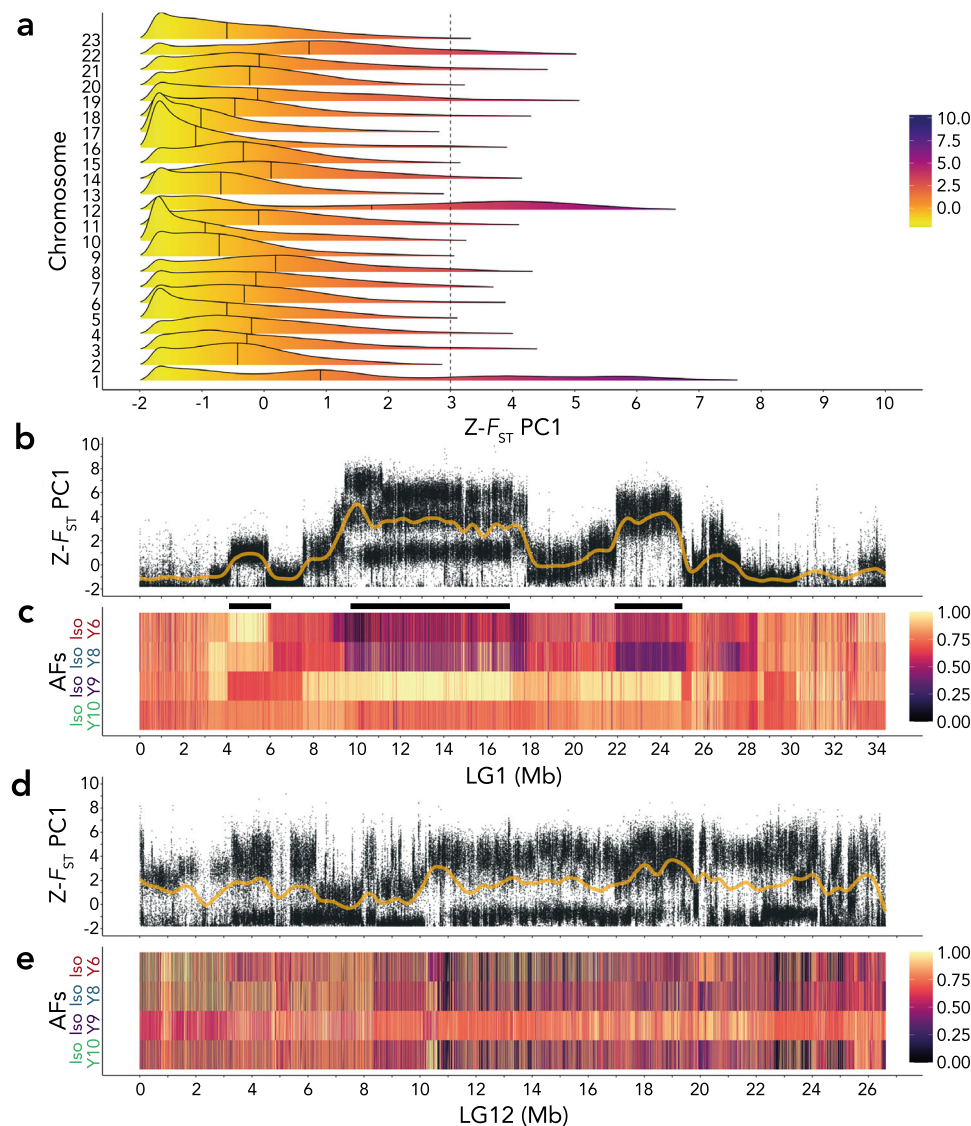


Fig. 2 Genetic differentiation between the four Iso-Y lines: Iso-Y6; Iso-Y8; Iso-Y9; Iso-Y10. **a** Density plots of the SNP distribution of $Z-F_{ST} PC1 F_{ST}$ for each chromosome of the guppy genome (23 chromosomes). The colour scale represents the $Z-F_{ST}$ scores as depicted in the legend (yellow: low-scoring SNPs; indigo: high-scoring SNPs). Black lines within each density curve mark the median value of each chromosome. Dashed x-axis intersect marks the upper 95% quantile of 3. **b** Per-SNP $Z-F_{ST} PC1$ scores for LG1; yellow line represents a smoothed spline of the data. **c** Allele frequency (AF) plots of LG1 for each Iso-Y line (Iso-Y6—red; Iso-Y8—blue; Iso-Y9—purple; Iso-Y10—green). AFs were polarised to the major allele of Iso-Y9. Changes in the AFs are represented by the colours depicted in the legend. On LG1, Change Point Detection (CPD) pinpointed three regions of consistent differentiation, which are indicated at the top by black rectangles: Region 1 (4–5.9 Mb); Region 2 (9.6–17 Mb); Region 3 (21.9–24.9 Mb). **d** Per-SNP $Z-F_{ST} PC1$ scores for LG12; yellow line represents a smoothed spline of the data. **e** Allele frequency (AF) plots of LG12 for each Iso-Y line. AFs were polarised to the major allele of Iso-Y9 and changes in the AFs are represented by the colours depicted in the legend. On LG12, Change Point Detection (CPD) did not uncover any consistent regions of differentiation between the Iso-Y lines. X ticks are displayed in Megabases (Mb). Source data underlying all components of Fig. 2 are provided as Source data files.

the allele frequencies (AFs—polarised to the major allele of Iso-Y9) and $Z-F_{ST} PC1$ (Fig. 2c). Region 1 encompassed ~ 1.9 Mb (coordinates: 4,079,988–5,984,584 bp). Region 2 encompassed ~ 7.4 Mb (coordinates: 9,627,619–17,074,870 bp). Region 3 encompassed ~ 3 Mb (coordinates: 21,944,840–24,959,750 bp). Using the same CPD methods, no regions were consistently differentiated between the Iso-Y lines on LG12 (Fig. 2e).

Next, to explore diversity within the Iso-Y lines, we calculated π across 10 kb windows for our two focal chromosomes (LG1 and LG12) and performed the same multivariate approach as above. On LG1, we found that regions of differentiation could be explained by a shared chromosomal landscape of diversity among all Iso-Y lines with $Z-\pi$ -LG1 PC1 (PC1 captured 74% of the

variance) accounting for the majority of variance in diversity (Supplementary Fig. 12; Supplementary Table 7). We found no evidence of increased coverage associated with increased diversity in the regions of LG1 (Supplementary Fig. 13). On LG12, $Z-\pi$ PC1 accounted for most of the variance (PC1 captured 88% of the variance) and showed a significant (>99% upper quantile of 4.6) peak in diversity at 24.27 Mb (Supplementary Fig. 14; Supplementary Table 8). $Z-\pi$ -LG12 PC2 (PC2 captured 7% of the variance) showed a high level of residual variance in π , associated with the variance of Iso-Y9, that was not otherwise explained by the general chromosomal landscape. The diversity hotspot (peak at 24.28 Mb, >99% upper quantile of -1.4) represented by PC2 is thus unique diversity within Iso-Y9. Both LG12 peaks: 24.27 Mb

(π shared by all Iso-Y lines); and 24.28 Mb (π unique to Iso-Y9) overlap with previously recorded high male diversity at the putative non-recombining Y³¹.

Evidence of multiple haplotypes and candidate colour genes on LG1. In Region 2 (9.6–17 Mb), two bands of F_{ST} were apparent in analysis of Z- F_{ST} -LG1 PCI, and in pairwise F_{ST} (Fig. 2b; Supplementary Fig. 7). To explore this further, we assessed the segregation of the AFs within each of the three identified regions in more detail (Supplementary Fig. 15). Corresponding to the double-banding of F_{ST} , Region 2 showed unusual AF patterns within the lines. Iso-Y9 showed fixation, but the other three Iso-Y lines showed multiple bands of AFs, which taken together did not sum to 1. Additionally, in Region 3, Iso-Y6 also showed two sets of distinct bands of AFs. Assessment of the AF density distributions showed clear patterns of bimodality (trimodality in Iso-Y6) in Region 2 (Supplementary Fig. 16) and bimodality in Iso-Y6 in Region 3 (Supplementary Fig. 17). The distinct patterning corresponding to the different bands of AFs could suggest strong linkage between the SNPs segregating in each band, indicative of multiple maintained haplotypes. We reasoned that a complex haplotype structure exists, in which alleles associated with more recently derived haplotypes are nested within an older haplotype (Fig. 3). Bimodal AF distributions parsimoniously represent AFs associated with the older (larger density peak) and younger, derived (smaller density peak) haplotypes.

We found several strong candidates for colour, male-specific fitness and vision in the three differentiated regions on LG1 (see Supplementary Data 1 for a full list of gene annotations).

Region 1 (4–5.9 Mb) contained 62 predicted genes. Of interest was *tll1*, with a role in caudal fin, dorsoventral patterning in *D. rerio*⁴³, *pcm1* involved in spermatogenesis⁴⁴, and *ptpn13* which is Y-linked in humans⁴⁵ and in some fish due to its physical linkage with *gsdf*, a gene which is highly conserved in fish sex differentiation pathways^{46,47}. Region 2 (9.6–17 Mb) contained 291 predicted genes. Genes with a potential role in colour included *xpa*, involved in pigmentation and photosensitivity to UV light⁴⁸, *pcdh10a* involved in melanocyte migration, *crebbpa*, which has been identified as a candidate for plumage colouration in chickens⁴⁹, and *shoc2*, which causes pigmentation abnormalities⁵⁰, as well as five keratin genes, which have a role in pigmentation⁵¹. We also identified five retinal genes (*slc24a2*⁵², *strab6*⁵³, *pnpla6*⁵⁴, *cabp2a*⁵⁵ and *nrx1*⁵⁶), and three genes involved in spermatogenesis or sperm motility (*tdrd7a*⁵⁷, *nanos3*⁵⁸ and *tekt4*⁵⁹). Region 3 (21.9–24.9 Mb) contained 94 predicted genes. This region also contained several promising candidates including two paralogs annotated as *kita*, previously identified as a key gene involved in pigment pattern formation in guppy strains⁶⁰ and zebrafish⁶¹, *sox10a*, a sex determining region Y-box that regulates the expression of the *mitf* gene, which is the master regulator of melanophore–melanocyte differentiation in teleosts⁶², and is also responsible for colouration in rock pigeons⁶³, *mchr1*, a melanin-concentrating hormone receptor, and a *TRYP*, located in melanocytes and involved in the production of melanin⁶⁴. We also performed an assessment of Gene Ontology (GO) enrichment and KEGG mapping for the three regions on LG1 (see Supplementary Data 2 for results). Analysis using gene annotation information combined across all three LG1 regions showed a significant KEGG mapping to Lysosome (11 genes). This is of potential interest given that the melanosome is a lysosome-related organelle.

Evidence for the LG1 haplotype in the natural population. We next examined natural data by performing whole-genome sequencing of 26 wild-caught guppies from the source

population ($n_{\text{females}} = 16$, $n_{\text{males}} = 10$, average coverage $\geq 13\times$, final dataset = 1,021,495 SNPs). Using multiple lines of evidence, we found a large haplotype on LG1 (11.1–15.9 Mb) segregating in the natural source population, which lies within ‘Region 2’ identified in the Iso-Y analysis (9.6–17 Mb). We term this area ‘Region 2-NP’ (Region 2 Natural Population) (Fig. 4).

Analysis of linkage disequilibrium (LD) on LG1 revealed an area of high linkage between 11,114,772 and 15,890,374 bp, where it was apparent that several overlapping linkage blocks exist (Fig. 4a). We also analysed patterns of LD for males and females separately and found that males exhibited at least two distinct neighbouring linkage blocks, but females showed high linkage across the entire region (Supplementary Fig. 18). We then assessed shifts in local ancestry by performing a local PCA approach⁶⁵, which recapitulated the identified areas of high LD (Fig. 4b), with a pattern of significant differentiation (saturated eigenvalues > 0.01) represented by three overlapping multidimensional scales (MDS) on LG1: MDS1: 11,216,906–15,375,083 bp; MDS2: 11,430,012–14,570,259 bp; MDS3: 12,326,328–15,308,055 bp. This demonstrates that subsets of correlated SNPs within Region 2-NP exhibit ancestry relationships that deviate from those observed across the rest of the chromosome; a pattern indicative of inversions, long haplotypes under balancing selection, reduced recombination, or changes in gene density⁶⁵.

Intersex F_{ST} showed differences between the sexes within Region 2-NP (Fig. 4c); in particular, an area of high density of elevated intersex F_{ST} between 12.2 Mb to 13.1 Mb. We found that elevated intersex F_{ST} was driven by a reduction in male-specific diversity, as measured by intersex D_a (D_{XY} - female π ; Fig. 4d). Overall, these results suggest that selection is operating differently between the sexes in the candidate region.

As recombination history is known to affect the maintenance of tightly linked genetic architectures⁶⁶, we also examined the genome features of Region 2-NP. We did not observe any differences in the proportion of GC content (Supplementary Fig. 19), nor repeat elements (Supplementary Fig. 20) in our candidate region. SNP density within Region 2-NP was considerably higher compared to the rest of the chromosome (Supplementary Fig. 21), but there was no evidence of extremes in read depth indicative of duplication or copy-number variation (Supplementary Fig. 22). Gene density showed a moderate number of genes across Region 2-NP, and a drop in gene density at ~13.2 Mb (Supplementary Fig. 23).

We performed similar analyses on LG12, confirming previously identified differences between the sexes^{30,31,35,67}. LD analysis showed two main regions of increased linkage; a fragmented region extending from 4.6 to 6.7 Mb, and another more clearly defined region near the terminal end of the chromosome (23.8–25.3 Mb) (Fig. 4e). A local PCA of LG12 identified two significant MDS axes (saturated eigenvalues > 0.01) approximately corresponding with the areas of high linkage (Fig. 4f). MDS1 outliers were observed at the terminal end of the chromosome (coordinates: 21,913,633–25,664,533 bp). MDS2 depicted an area encompassing the latter part of the high linkage block, extending past it in the latter coordinates (coordinates: 5,608,703–7,063,435 bp; Fig. 4e).

Overlapping with MDS2, a significant elevation in intersex F_{ST} was observed (Fig. 4g) and in the latter part of the region, a narrow peak in significantly increased male diversity was detected at 5.67 Mb (Fig. 4h). This second region overlaps with a previously identified D_a outlier window in an analysis of six natural populations (6.94–6.95 Mb and 7.00–7.01 Mb), where male-specific D_a was notably higher in high-predation (HP), compared to low-predation (LP) populations³¹. Moreover, the LD in this region extends across 4.6–6 Mb which includes another previously identified male-biased candidate region (LG12:

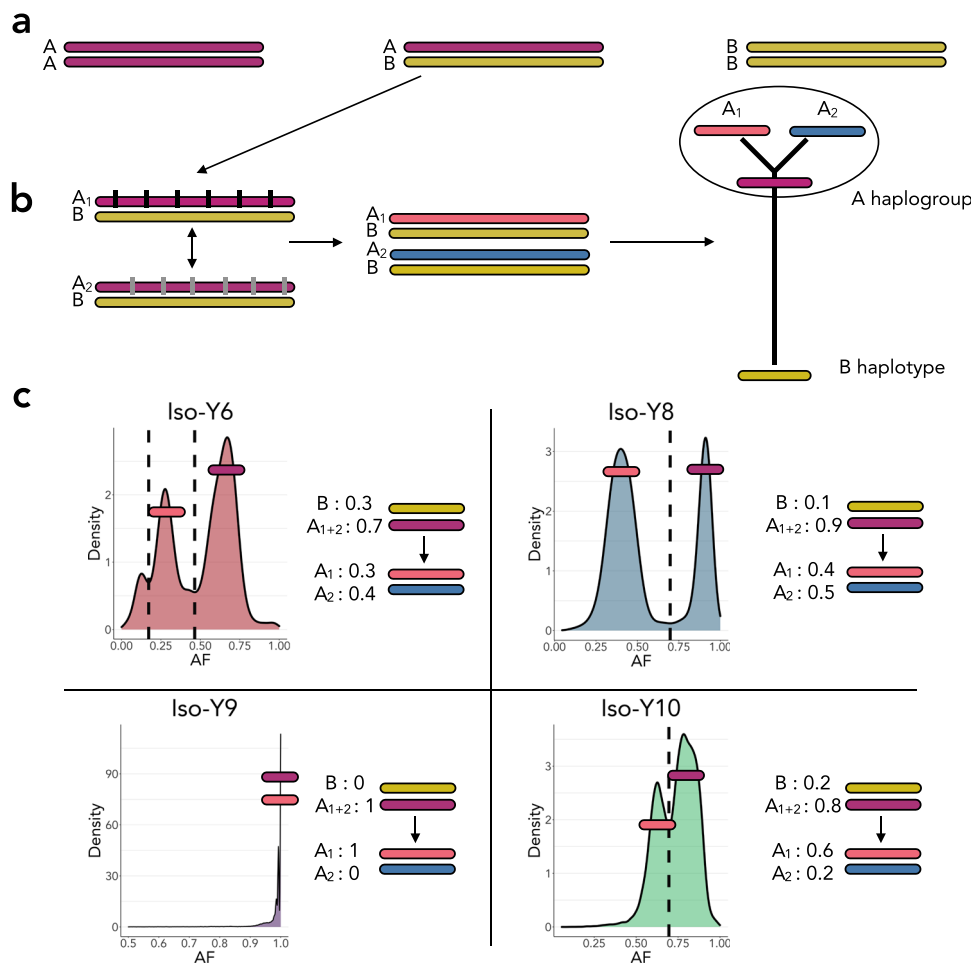


Fig. 3 Schematic representation of the multiple bands of allele frequencies present in the Iso-Y Pool-seq data. **a** AA represents homozygous, AB represents heterozygous, and BB represents homozygous alternative. **b** The ancestral A haplotype accumulates SNPs, differentiating it into two versions of the A haplotype: A1 and A2. The ‘Y’ shaped haplotype tree represents the predicted evolutionary relationships between the ‘A haplogroup’ composed of ancestral A, derived A1 and A2 haplotypes, and the ‘B haplotype’. Branch lengths represent evolutionary distance, and thus SNP count. We predict that Iso-Y9 is fixed for one of the derived A haplotypes. For illustration purposes, we have shown fixed allele frequencies (AFs) for the A1 haplotype. The remaining Iso-Y lines are all heterozygous with the AB genotype. There are no BB individuals. Individuals within the Iso-Y6, Iso-Y8 and Iso-Y10 pools have segregating A1 and A2 haplotypes, which when compared to Iso-Y9 A1 show multiple bands of AFs, as shown in the AF calculations in part (c). Due to the nature of Pool-seq, it is unclear what the actual genotypes are. We focus on providing an explanation of the bimodal peaks, but it is noteworthy that in Iso-Y9 there are many fixed sites, but also some ‘nearly fixed’ sites, which suggests some diversity also exists in the Iso-Y A1/A1 haplotype, which likely represents the trimodality of Iso-Y6, (i.e. further complexity in the A1/A1 haplotype that’s captured in comparisons with Iso-Y6). Refer to Supplementary Figs. 16 and 17 for further visualisation of the segregating AFs.

4.8–5.2 Mb)³¹. An assessment of the gene annotations within the MDS2 coordinates identified only a few candidates of interest (Supplementary Data 3): *dmgdh*, a gene that affects sperm trait variation and is part of a sex-supergene in songbirds⁶⁸ and *bhmt*, a folate-related gene that shows an association with skin pigmentation in humans⁶⁹.

It is predicted that the terminal region of LG12 contains the sex-determining locus (SDL)^{28,70,71} and a recent multiple population genomics survey identified a sex-linked region between 24.5 and 25.4 Mb in LG12, which overlaps with the region of high LD and MDS1 region identified here³¹. Moreover, analysis of intersex F_{ST} showed high differentiation between the sexes in the region (Fig. 4g), and analysis of intersex D_a revealed that this was driven by an excess of male diversity (Fig. 4h). In contrast to LG1, which showed that elevated intersex F_{ST} was driven by reduced male diversity, the high diversity observed here is consistent with a hypothesis of multiple diverse Y-haplotypes and NFDS on the Y³⁵. Previous investigation of the gene content within the terminal region found it to be relatively gene-poor,

containing multiple repeated copies of NLRP1-related genes³¹, which form part of the inflammasome⁷² and have no known role in sex determination. Our analysis of gene content for the slightly expanded region found in this population identified a single potential colour pattern candidate (*vldlr*), which is responsible for caudal fin patterning in *Danio rerio*⁷³, and two male-trait candidates: *AIG-1* (androgen-induced protein-1) family, and *spag16* (sperm-associated antigen 16) (Supplementary Data 3).

Pinpointing informative breakpoints within the LG1 haplotype. Combining both the natural population data and our experimental Iso-Y lines, we found evidence for the maintenance of a large, highly diverse haplotype on LG1 associated with male-specific colour. In the Iso-Y lines, Region 2 encompassed multiple bands of tightly associated allele frequencies, suggesting multiple derived haplotypes. Analysis of the natural population data revealed that Region 2-NP is characterised by elevated linkage, and is defined by linkage patterns indicative of not just one, but multiple derived local ancestries. Comparisons of male and

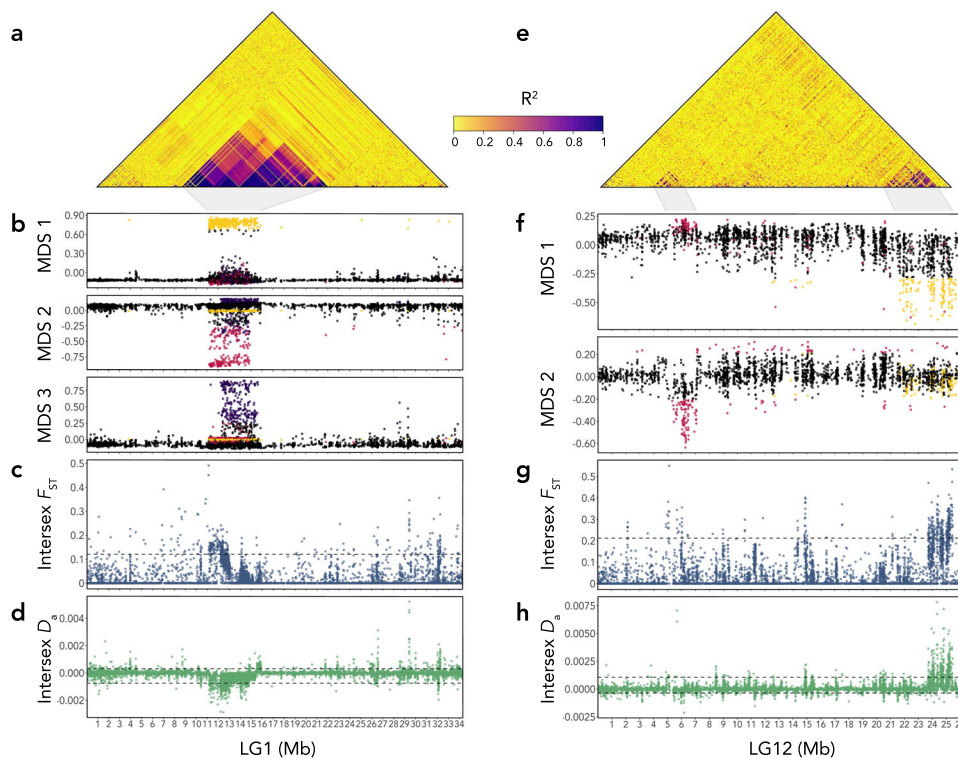


Fig. 4 Analysis of LG1 and LG12 in the natural source population ($n_{\text{females}} = 16$, $n_{\text{males}} = 10$). **a** LG1 heatmap of patterns of linkage disequilibrium (LD) measured as R^2 . Amount of LD is shown by colour intensity as depicted in the legend (yellow: low LD; indigo: high LD). High LD is observed at coordinates: 11,114,772–15,890,374. **b** LG1 local PCA in 10 bp windows, depicting three significant multidimensional scales (MDS): MDS1 (yellow, coordinates: 11,216,906–15,375,083 bp); MDS2 (pink, coordinates: 11,430,012–14,570,259 bp); MDS3 (purple, coordinates: 12,326,328–15,308,055 bp). **c** Intersex F_{ST} calculated in 1 kb windows across LG1. Dashed line marks the 95% quantiles. **d** Intersex D_a calculated in 1 kb windows across LG1. Dashed lines mark the 5% and 95% quantiles. **e** LG12 heatmap of patterns of linkage disequilibrium (LD) measured as R^2 . Amount of LD is shown by colour intensity as depicted in the legend (yellow: low LD; indigo: high LD). High LD is observed between -4.6–6 Mb and at the terminal region between -23.8–25.3 Mb. **f** LG12 local PCA in 10 bp windows, depicting two significant multidimensional scales (MDS): MDS1 (yellow, coordinates: 21,913,633–25,664,533 bp); MDS2 (pink, coordinates: 5,608,703–7,063,435 bp). **g** Intersex F_{ST} calculated in 1 kb windows across LG12. Dashed line marks the 95% quantile. **h** Intersex D_a calculated in 1 kb windows across LG12. Dashed lines mark the 5% and 95% quantiles. X ticks are displayed in Megabases (Mb). Source data underlying all components of Fig. 4 are provided as Source data files.

female diversity within the population suggests selection may operate differently between the sexes in Region 2-NP; in particular, between 12.2 Mb and 13.1 Mb, which showed high intersex F_{ST} and a reduction in male diversity. Structural variant (SV) analyses using short-read and long-read data did not show support for SVs in Region 2 nor Region 2-NP (Supplementary Data 4). Our prediction is that the region encompasses a large and diverse haplotype, and that within this haplotype, genetic rearrangements have resulted in several derived haplotype segments. To interrogate this further, we performed an in-depth analysis.

Individual genotypes of the Iso-Y lines and the natural population data across LG1 revealed long stretches of maintained genotype states within Region 2-NP (Fig. 5a). In the Iso-Y line data, Iso-Y9 showed distinct blocks of fixed HOM ALT genotypes, whilst the other Iso-Y line genotypes were entirely heterozygous (HET). This observation is congruous with the multiple bands of allele frequencies observed in the Iso-Y line data. Of individuals from the natural population ($n_{\text{total}} = 26$), 17 ($n_{\text{females}} = 10$, $n_{\text{males}} = 7$) shared the same overall genotype signature of HOM ALT genotype blocks as seen in Iso-Y9. Seven individuals ($n_{\text{females}} = 4$, $n_{\text{males}} = 3$) showed genotype blocks alternating between areas with the Iso-Y9 HOM ALT genotype signature, and areas of heterozygosity. Lastly, only two individuals showed a signature of extended blocks of HOM REF genotypes:

NAT08 and NAT16 ($n_{\text{females}} = 2$, $n_{\text{males}} = 0$), yet HOM REF genotypes were only maintained for a proportion of the entire region.

By phasing the heterozygous individuals ($n_{\text{total}} = 9$), we found evidence of two large divergent haplotypes encompassing the entirety of Region 2-NP with subsequent recombination at conserved breakpoints (Fig. 5b). This indicates that the whole high linkage block is not one large inversion. We identified six repeated breakpoints (i.e. occurring in ≥ 2 individuals): BP1: 11.6 Mb ($n_{\text{females}} = 2$); BP2: 11.7 Mb ($n_{\text{females}} = 3$); BP3: 12.2 Mb ($n_{\text{females}} = 3$, $n_{\text{males}} = 1$); BP4: 13.1 Mb ($n_{\text{females}} = 2$, $n_{\text{males}} = 2$); BP5: 14.4 Mb ($n_{\text{females}} = 2$); BP6: 15.4 Mb ($n_{\text{females}} = 2$).

These analyses allowed us to pinpoint breakpoints contributing to patterns of differential selection and linkage between the sexes. From the start of Region 2-NP to BP3 (12.2 Mb), there was a distinct difference in zygosity between males and females (Females: 11 HOM ALT, 4 HET, 1 HOM REF; Males: 10 HOM ALT). Therefore, males are out of HWE; based on the female AFs, we would expect 5 HOM ALT, 3 HET and 2 HOM REF in males. The region delineated by BP3 to BP4 overlaps with a high density of SNPs showing signatures indicative of sex-differential selection (12.2 Mb to 13.1 Mb). The only breakpoint consistent between males and females (BP4) also distinguishes the break in LD in males, the drop in gene density, and a break in derived ancestry estimates of 100 bp windows (Supplementary Figs. 18, 23, 24).

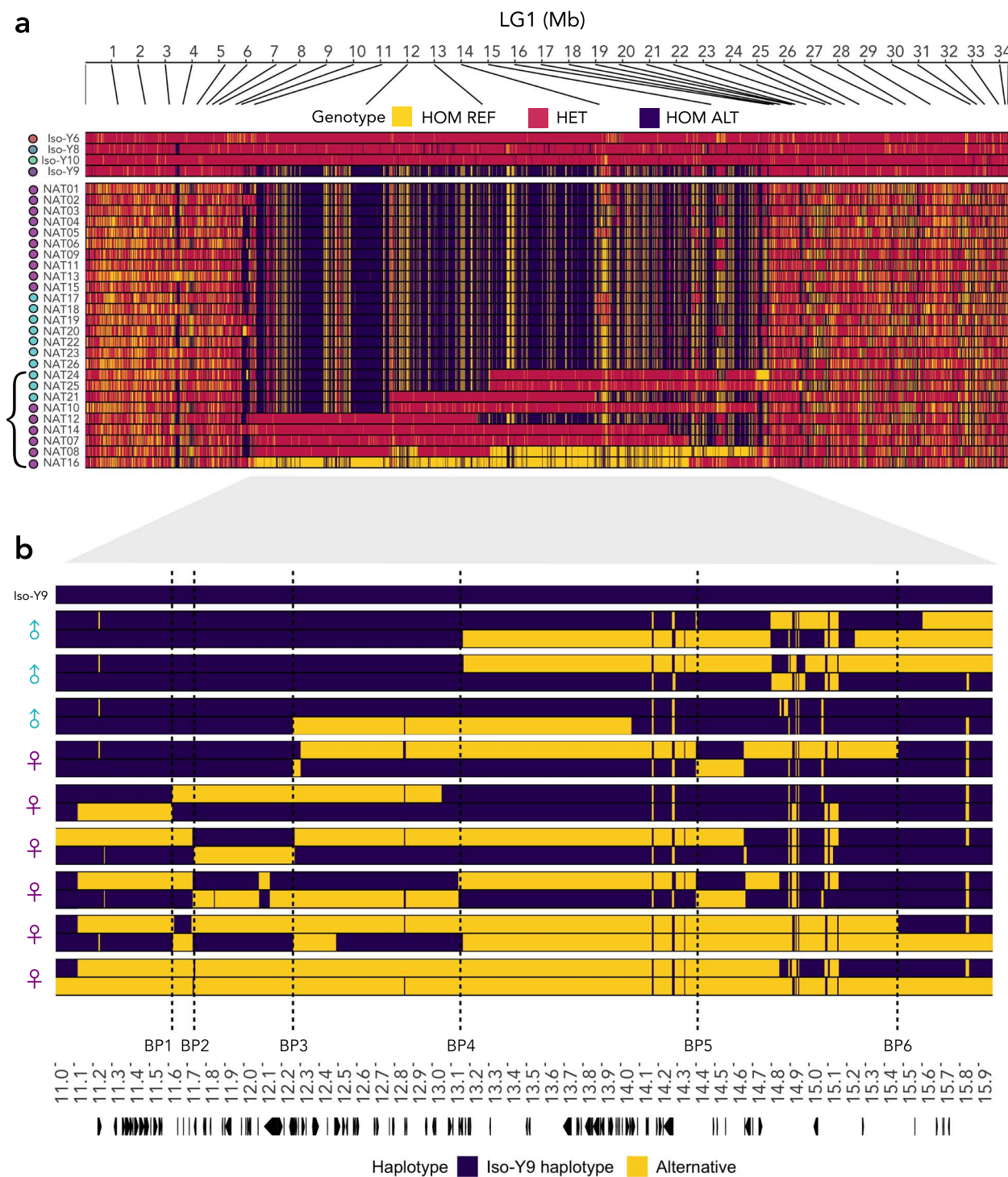


Fig. 5 LG1 Region 2 haplotype structure. a Genotype plot for Iso-Y lines and natural data combined showing the genotype of each SNP depicted as homozygous reference (HOM REF: yellow), heterozygous (HET: pink) or homozygous alternative (HOM ALT: purple); each individual is coloured by Iso-Y line, or by sex (females in purple, males in cyan). The bracket shows the heterozygous individuals used in the haplotype analysis in panel (b). **b** Haplotype plot of phased data for natural-derived heterozygous samples ($n_{total} = 9$, $n_{males} = 3$, $n_{females} = 6$) polarised to the Iso-Y9 haplotype (purple) and alternative haplotype (yellow). Symbols next to each of the individuals represent sex (females in purple, males in cyan). Breakpoints (BP) in the haplotype are identified when phases switch between purple and yellow. Dashed lines mark conserved BPs (≥ 2 individuals): BP1: 11.6 Mb ($n_{females} = 2$); BP2: 11.7 Mb ($n_{females} = 3$); BP3: 12.2 Mb ($n_{females} = 3$, $n_{males} = 1$); BP4: 13.1 Mb ($n_{females} = 2$, $n_{males} = 2$); BP5: 14.4 Mb ($n_{females} = 2$); BP6: 15.4 Mb ($n_{females} = 2$). Arrows at the bottom highlight the location of gene annotations for the region. Source data underlying all components of Fig. 5 are provided as Source data files.

Taken together, this localises our candidate region from the beginning of Region 2-NP to BP4 as both selected in males in a natural population and associated with colour in our breeding design.

Discussion

Overall, our results reveal a surprising genetic architecture for colour pattern diversity in guppies. Even though the differences in colour pattern between the Iso-Y lines are Y-linked (i.e. inherited faithfully from father to son), consistent genetic differences are most pronounced on an autosome, LG1. Analysis of the phenotype data showed that the breeding design was successful in producing four distinct Iso-Y lines with marked differences in colour pattern. Using these unique Iso-Y lines, we delineated three regions on LG1 that were consistently different among the differently coloured lines, and within these regions we identified many genes known to be linked to colour in model species. Then, using extensive WGS from the source population, we further highlight just one of these regions (Region 2-NP: 11.1–15.9 Mb), as having strong linkage and significant local ancestry, finding that a large and variable haplotype is maintained in nature.

We had hypothesised that the Y-linked colour pattern genes in our Iso-Y lines would be located on the sex chromosome, LG12. If colour pattern traits are fully Y-linked, and each Iso-Y line's unique Y haplotype is fully inherited through the patriline, then with this breeding design we would predict a consistent pattern of high differentiation in the Y-linked region on LG12 between all Iso-Y line comparisons. Instead, we see that overall, the chromosome shows moderate divergence, driven by elevated differentiation in comparisons to Iso-Y9 and localised regions of differentiation in comparisons with Iso-Y6. Whilst elevated F_{ST} across the chromosome is expected due to sex linkage, we found no evidence of a consistently differentiated region on LG12. Moreover, all guppy chromosomes are acrocentric and show evidence of male heterochiasmy^{30,67,74}; yet recombination events are particularly rare on LG12, implying that LG12 may decompose at a slower rate compared to autosomes. Our LG1 haplotype on the other hand, shows consistent differentiation between the lines. The near fixation of the LG1 Region-2 haplotype between the lines is strong evidence for this region harbouring genes involved in colour.

An alternative explanation for the association between LG1 Region-2 haplotype and colour is unusually low recombination on LG1 and insufficient backcrossing, resulting in a spurious relationship. However, we think this scenario is unlikely; there is no evidence of unusually low recombination on LG1^{30,33} (Supplementary Fig. 9), and as each generation reduces the proportion of parental genome by half, just <0.01% of the parental genome should remain after 13–20 generations of backcrossing. Moreover, we found that Iso-Y6 and Iso-Y8 are the least phenotypically divergent lines, and they also showed the lowest genetic differentiation on LG1.

Our hypothesis is that colour pattern is controlled by the epistatic interaction between Y-specific regions and our candidate region on LG1 in this population. Y-autosome epistasis has been reported previously in other systems. For example, polymorphisms on the gene-poor Y chromosome in *Drosophila* spp. have been shown to differentially affect the expression of hundreds of X-linked and autosomal genes, specifically those that are highly expressed in males, and with clear fitness-related functions in males (e.g. spermatogenesis and pheromone detection^{75,76}). Previous research on this population of guppies (Paria) also supports our working hypothesis. Testosterone-treated females from Paria displayed high amounts of colour, suggesting an

autosomal component to colour expression⁷⁷. However, it has also been found that males in Paria exhibit strong patrilineal inheritance of colour pattern, suggesting the importance of the Y³⁶. Given the success of our breeding design, where introgressed Iso-Y lines were significantly different in colour, we also found strong evidence for Y-linkage for colour. Ongoing work is directly testing the roles of Y-autosome epistasis versus Mendelian inheritance on guppy colour pattern by conducting crosses between Iso-Y lines with different LG1 haplotypes. Furthermore, it would be interesting to quantify the colour patterns of testosterone-treated females derived from these lines to more fully explore inheritance patterns in females.

By further exploring our natural source population data, we can begin to hypothesise how this epistatic interaction might operate and how it may lead to the maintenance of Y-linked variation in colour. We recorded differences between the sexes in LG1 Region 2-NP, although this region did not appear in a previous analysis examining consistent differences between the sexes across multiple populations³¹. We found that this difference is caused by a reduction in expected diversity in males, where males were not in HWE in the region from 11.1 Mb to 13.1 Mb (start of Region 2-NP to BP4), although females were in HWE. This could be indicative of a deleterious Y-autosome interaction, where certain Y haplotypes are incompatible with the 'REF' LG1 haplotype. Guppy adult sex-ratios, are indeed, generally female-biased^{78–81}, and show a stronger female-bias in upstream low-predation (LP) environments, like Paria, albeit with sampling variability^{78,81}. We found no evidence for large structural rearrangements (such as inversions) underlying the maintenance of our candidate region, LG1 Region 2-NP, and did not detect any relationship with our predicted conserved recombination points, nor increased GC or TE content. Therefore, exactly which molecular traits are driving this haplotype structure is unclear. By examining phased heterozygous individuals, it is however, apparent that crossing-over is restricted to key points along the haplotype and overall linkage is maintained in the population. Models of balancing selection show that balanced variants produce diversity patterns similar to those caused by positive selection⁸², and simulations suggest that balancing selection alone can maintain high-LD, and in particular, high divergence between colour phenotypes⁸³. Taken together, our natural source population data reveals interesting signals in this region but determining the selective forces responsible for its maintenance requires a larger sample size, and colour pattern phenotype data from the natural source population, particularly for recombinant males.

It has been argued that selection must be extremely strong, or unrealistic, for differences in allele frequencies to be maintained between the sexes on an autosome^{84,85}. On the other hand, it is also contended that sex differences on autosomes are artefacts caused by duplications or translocations onto the Y chromosome⁸⁶. Read coverage was not increased in the LG1 region, and we found no evidence of reduced mapping quality, which would be expected if this region was the result of a duplication or translocation event. Nor do we find evidence that our candidate region on LG1 is misassembled; we previously found strong Hi-C contact across the chromosome, although the genome assembly is derived from an individual from a different population³¹. We also found no evidence that a translocation from LG1 to LG12 had occurred uniquely in this population in our SV analyses, and we did not observe elevated inter-chromosomal LD in the natural data (Supplementary Fig. 25). Moreover, linkage along chromosomes, including LG1, has been observed in several different populations and mapping crosses suggesting a translocation is unlikely to be the cause^{30,33,67}. We

do however recognise that evolution of sex determination mechanisms and sex chromosomes have occurred in laboratory-adapted populations in a similar number of generations, in both *Danio rerio*⁸⁷ and *Xiphophorus*⁸⁸.

Early research found that the linkage between colour pattern traits and the Y was under selection, with increased Y-linkage for colour traits in downstream, high-predation (HP) environments and X-linkage in the upstream, low-predation (LP) environments. Whether Y-linkage varies by predation environment has been indirectly studied across Trinidad, where females treated with testosterone exhibited more colour patterns in LP populations compared to their HP counterparts^{77,89}. Such observations are also consistent with an autosomal genetic component of colour pattern traits that are under weakened selection in LP environments⁹⁰. Other studies suggest that the size of different strata on LG12 vary between HP and LP, with increased Y-linkage in LP³⁴ (see also^{35,91}), but these results were not repeated across other HP-LP pairs^{30–32}. Our candidate region on LG1 may explain differences in Y-linkage between predation ecotypes. Specifically, we identified a region between 12.2 Mb to 13.1 Mb with reduced diversity in males, compared to females, which also corresponded with a break in male patterns of LD. Previous analysis of molecular convergence between HP and LP populations identified two outlier windows in this area (12.17–12.18 Mb and 12.21–12.2 Mb), indicating that this particular region may be under divergent selection for HP-LP phenotypes⁹². We further compared WGS data from other populations across Trinidad at LG1, and detected a strong signal of HP-LP association within 12.2 Mb to 13.1 Mb, but the large haplotype structure is unique to the population studied here (Supplementary Fig. 26). This suggests that this region may be involved in the differential selection of colour phenotypes depending on predation regime.

Based on our Iso-Y lines and natural population data, we hypothesise a Y-autosome epistatic genetic architecture for guppy colour traits. This architecture may be particularly well-suited to a Y-linked trait under NFDS, such as guppy colour pattern. Models suggest that sex-linked polymorphism can only be maintained by natural selection in unusual genetic systems, where the maintenance of Y-linked variation in Y-autonomous models involves frequency-dependent selection, or interactions with other chromosomes⁹³. Recognition of the importance of epistasis in response to selection is growing, and epistasis may be responsible for an increased, or non-linear rate, of adaptation in natural populations or artificial selected lines⁹⁴. Additionally, having loci under NFDS not physically linked to the Y can shield them from increased drift experienced on the Y, allowing for higher levels of variation to be maintained⁹⁵. Finally, for NFDS to operate, we would hypothesise that there should be a balance between keeping coadapted alleles together and breaking them apart to create variation. Together, this suggests that Y-autosome epistasis acting on a diverse autosomal haplotype presents a feasible hypothesis for the maintenance of colour pattern traits. The Iso-Y lines offer a unique resource to explore interactions between LG1 and LG12, and also to further distinguish the role of the three different regions on LG1 by performing focussed crosses between Iso-Y lines. Future studies should also aim to fully characterise the diversity of LG1, including additional long-read sequencing of multiple individuals from both LP and HP environments in order to determine the reservoir of variable haplotypes present in this region.

Methods

Generation of the Iso-Y lines. All procedures involving live animals were reviewed and approved by the Florida State University Animal Care and Use Committee (protocol no. 1442 and no. 1740). The Iso-Y lines were kindly provided

by AE Houde, who established them by choosing male lineages in which colour pattern on the body was strongly Y-linked. Each line was founded by a single male drawn from the ‘Houde’ tributary of the Paria River in Trinidad (Trinidad National Grid System: PS 896886). Males from this tributary are known to show strong Y-linkage¹⁹. Each Iso-Y line was maintained by breeding males with colour patterns similar to that of each line’s founder; hence, the colour patterns of the Iso-Y lines are ecologically relevant. Every generation, males were mated to females sired by males from the same line, or, every 2–3 generations, backcrossed into the stock population derived from the same Houde tributary. The lines have been maintained at Florida State University since 2012.

Colour pattern phenotype analysis

Photography. We used multispectral digital photography (Sony A7 with full-spectrum conversion; Nikon 80 mm f/5.6 El-Nikkor Enlarging Lens) to capture human-visible and ultraviolet images of males from each Iso-Y line (Iso-Y6_n = 41; Iso-Y8_n = 48; Iso-Y9_n = 42; Iso-Y10_n = 42). Fish were lightly anaesthetised by immersion in a Tricaine mesylate (Pentair) solution and placed on a clear petri dish above a grey background with the left side of the body facing upwards. A soft tip miniature paint brush was used to raise the dorsal fin, flare the caudal fin, and lower the gonopodium so that these appendages were visible. Fish were illuminated by four metal halide lights (Hamilton, 6500 K bulbs) that simulate the natural photic environment. A size standard and two full-spectrum colour standards (grey—20% reflectance, white—99% reflectance; Labsphere) were included beside the fish. Glare and shadow were minimised by placing a diffuser (cylinder of 0.015” polytetrafluoroethylene) around the fish and colour standards. We photographed each fish once in the human visible spectrum (Baader UV/IR cut / L-Filter) and once in the UV spectrum (Baader U-Venus-Filter 350 nm).

Morphometrics. Morphometrics were performed using the TPS Series software⁹⁶, using tpsUtil v1.81. We used tpsDig2 v2.31⁹⁷ to set the image scale using the size standard, and to place landmarks around the perimeter of the fish. Following Valvo et al.³⁹, we placed seven traditional landmarks at the tip of the snout, the anterior dorsal fin attachment, the posterior dorsal fin attachment, the dorsal caudal fin attachment, the ventral caudal fin attachment, the posterior gonopodium attachment, and the anterior gonopodium attachment. We then placed 55 semi-landmarks at approximately even intervals between the traditional landmarks. We used sliding of semi-landmarks to minimise any shape variation resulting from unequal distribution of semi-landmark placement. Next, tpsSuper v2.05⁹⁶ was used to generate a consensus shape representing the average shape of the males in all 346 photos (173 males * 2). Images of each individual were unwarped to this consensus shape, thereby mapping every pixel from the original image to an analogous location on the consensus shape.

Colour measurement. Analysis using Colormesh v2.0³⁹ was performed in R v4.0.2. We first performed Delaunay triangulation, which is used to reconstruct a complex shape (i.e. the shape of the unwarped fish) using a concise number of points distributed across the surface of that shape. We then measured the average colour of pixels in a radius around each of these sample points. We used cross-validation to determine the optimal number of Delaunay triangulations (more triangulations result in more granular colour pattern data) and sample circle radius (see below). At each sample point, we extracted linear colour measurements for four colour channels: R (red), G (green), and B (blue) and UV. We accounted for any minor fluctuations in the lighting environment by calibrating the colour values for each channel by subtracting the average deviation of colour measured in the photo on the white and grey colour standards from the known reflectance values of those standards.

Colour pattern differences among Iso-Y lines. We used Discriminant Analysis of Principal Components (DAPC) to describe the properties of colour pattern as this analysis is recommended for characterising the properties of groups using high dimensional data sets. We used the dapc function in adegenet v2.1.3⁴⁰ to perform a Principal Components Analysis (PCA), followed by a discriminant analysis to define the linear combinations of PC scores that minimise within and maximise between group variances.

We used DAPC in a cross-validation framework to determine the scheme for capturing colour data that allowed us to best discriminate among the Iso-Y lines³⁹. We used cross-validation to determine the optimal number of PC’s to retain, number of Delaunay triangulations to perform, and sample circle radius. Using the xvaldapc function, we performed DAPC on training and validation data, and examined the average proportion of successful assignments for a varying number of retained PC’s. We defined the training and validation populations each as 50% of the individuals from each line. We set the maximum number of PC’s to retain for cross-validation as $n.pca = 173$ (the number of fish), with cross-validations performed at 17 different retention levels in increments of 10 PC’s (up to 170). We performed 100 replicates per PC retention level. The average proportion of successful placements was maximised (at 98.8% successful) by retaining 10 PC’s, using four Delaunay triangulations, and a sample circle radius of one pixel. Consequently, we used this sampling scheme to measure colour pattern for all phenotypic analyses, retaining 10 PC’s for DAPC. This scheme resulted in 9904

colour measurements per fish (four colour channels * 2476 sampling locations), with colour averaged over 5 pixels per sample point.

To visualise the colour variation summarised by the discriminant functions, we generated heat maps depicting the correlations between position on each discriminant function and colour for each colour channel at each sampling location.

Comparing colour pattern differences among Iso-Y lines. To determine whether the Iso-Y lines have robust phenotypic differences, we used a permutational MANOVA to compare mean colour measures among lines. We first reduced the dimensionality of the colour pattern data for this analysis using PCA. We retained the first 17 PC's to summarise the greatest amount of variation in the data while keeping the ratio of observations to variables greater than 10:1 for our subsequent multivariate analyses. These PC's together explained 59.3% of the total variation in colour measurements. We then compared PC scores among lines using the adonis function in *vegan* v2.5-6⁹⁸, which computes the pairwise distances among observations and then performs a permutation test (randomly assigning labels among factors) to partition the distance matrix among sources of variation. P-values were then calculated using two-sided pseudo-F ratio tests. We used Euclidean distance and created 10 000 permuted samples per test. We additionally visualised the differences in phenotype among Iso-Y lines by generating density plots of each Iso-Y line for all 17 PC's used in permutational MANOVA (Supplementary Fig. 2).

Comparing colour pattern variance among Iso-Y lines. To quantify total within-line variance in colour pattern, we calculated the trace of the variance-covariance matrix among fish within a given line (across all colour channels and sampling locations). We then used permutational t-tests to determine whether phenotypic variance differed between each pair of lines, using the sample function. We permuted the line labels for each whole-fish colour pattern, thereby accounting for the fact that different colour measures on the same fish are not independent of one another. We created 10 000 permuted samples per test and performed two-tailed tests.

Genomic library preparation and variant genotyping

Pool-seq of the Iso-Y lines. Genomic DNA was extracted from 48 males of each Iso-Y line using an ammonium acetate extraction method from caudal peduncle⁹⁹. DNA quality was assessed using gel electrophoresis and DNA concentration calculated using Quant-iT Picogreen dsDNA reagent (Invitrogen) on a Glomax Explorer Microplate reader (Promega). DNA of each individual was diluted to 18–22 ng/μl and 4 μl of each added to a pooled sample per Iso-Y line. Pools were cleaned using a NEB Monarch clean up kit, with final concentration and quality of each confirmed using a Nanodrop ND-1000 (Thermo Fisher) and a Bioanalyser (Agilent). Library preparation and sequencing was performed at the University of Exeter Sequencing Service, using a NextFlex RAPID PCR-free library preparation protocol. Each of the libraries were sequenced across multiple lanes on a HiSeq 2500 in standard mode, with a 125 bp paired-end metric (Supplementary Table 9).

Raw reads were cleaned using *cutadapt* v1.13¹⁰⁰. Reads were aligned to the guppy genome³¹ (https://www.ebi.ac.uk/ena/browser/view/GCA_904066995) with *bwa mem* v0.7.17¹⁰¹ and converted to sorted bam alignment format with *samtools* v1.9¹⁰². Coverage was calculated using *qualimap* v2.2.1¹⁰³. Variants were called using *Freebayes* v1.3.1¹⁰⁴ with GNU parallel¹⁰⁵ by chunking the alignment files into regions based on coverage using *sambamba* v0.7¹⁰⁶. *Freebayes* was run with the options: `--use-best-n-alleles 4 -g 1000`. The raw variant output was filtered for bi-allelic SNP variants at QUAL > 30 and DP > 10, followed by a maximum missing filter of 80% applied to each pool separately followed by the application of a minor allele frequency (maf) of 25% applied across all pools using *vcftools* v1.9¹⁰⁷. The VCF file was used as input to *poolstat* v1.2¹⁰⁸, where the variants were filtered to exclude sites at <30× minimum coverage and <500× maximum coverage per pool, with a minimum read count per allele of 10 (Final SNP set = 3,995,905 SNPs). We used the curated liftover for LG12 for all analyses and plots of LG12¹⁰⁹.

Whole-genome sequencing (WGS) of wild-caught individuals. For the WGS of 26 wild-caught guppies, we sequenced individuals from the Paria river ($n = 9$) and used these with previously available data³¹ (Supplementary Data 5). Genomic DNA was extracted using the Qiagen DNeasy Blood and Tissue kit (QIAGEN, Cat No./ID: 69506). DNA concentrations ≥ 35 ng/μl were normalised to 500 ng in 50 μl and were prepared as Low Input Transposase Enabled (LITE) DNA libraries at The Earlham Institute, Norwich. LITE libraries were sequenced on an Illumina HiSeq4000 with a 150 bp paired-end metric and a target insert size of 300 bp, and were pooled across several lanes so as to avoid technical bias with a sequencing coverage target of $\geq 10\times$ per sample. Data from the LP Marianne river was previously generated ($n = 17$)³¹. Although the Paria and LP Marianne guppies are sampled from different sites, there is strong evidence that gene flow occurs between the populations occupying the upper reaches of these rivers^{110,111}. We found that genome-wide mean F_{ST} calculated between populations in this dataset was 0. Importantly, there was no effect of river on haplotype structure (Supplementary Data 5). Data processing followed previous methods using *GATK4* v4.1.8.1¹¹². Final filtering of the VCF file included filtering for bi-allelic SNPs at a minimum depth of 5 and a maximum depth of 200, removing 50% missing data and application of a 10% maf filter (Final SNP set = 1,021,495). Variants were phased

individually with *Beagle* v5.0¹¹³, and then phased again using *Shapeit* v2.r904^{114,115} making use of phase-informative reads (PIR)¹¹⁶. We used the curated liftover for LG12 for all analyses and plots of LG12¹⁰⁹.

Long-read sequencing. To assist with the phasing of variants called from short-read data and to detect structural variants (SVs) we generated 20 Gb of long-read Pacbio data from one of the Iso-Y individuals (Iso-Y6). High molecular weight DNA was extracted using DNeasy Blood & Tissue Kit (QIAGEN, Cat No./ID: 69506) with modifications (10× Genomics Sample Preparation Demonstrated Protocol and MagAttract HMW DNA Kit handbook). Data were sequenced on 3 SMRT cells of a PacBio Sequel at the University of Exeter Sequencing Service. For phasing, reads were aligned to the guppy genome using *minimap2* v2.17¹¹⁷. Genotypes were phased using *whatshap* v0.18¹¹⁸ using the reference genome and the long-reads to lift phasing information.

Analysis of Iso-Y-line genomic data.

Analyses were conducted in R v4.0.1. Pairwise F_{ST} was calculated using the Anova F_{ST} method implemented in *poolstat* v1.2¹⁰⁸. Per SNP F_{ST} values were compared pairwise between each Iso-Y line. To identify chromosomes with the highest mean variance in F_{ST} differentiation across our dataset, mean Z-scores of each PC were summarised for each chromosome⁴². These were calculated using the *prcomp* function using *stats* v3.6.2, centering and scaling the results.

To delineate line-specific blocks apparent from the distinct patterns of differentiation observed in the F_{ST} analysis, we evaluated the allele frequencies (AFs) of each line. AFs were extracted from the Pool-seq object generated by *poolstat* and were polarised to Iso-Y9 (the line which showed the highest genetic differentiation). To explore delineation breakpoints in the AFs, we adopted the use of change point detection (CPD) analysis. CPD was conducted in R using *changept* v2.2.2¹¹⁹. We used individual AFs from each Iso-Y line as input to detect mean changes, using the *BinSeg* method and SIC criterion. The number of changepoints identified is Q; in cases where several change points were detected, we increased the value of Q to 10. To add support to the change points detected using the AFs, and to ensure we were not missing any additional breakpoints, we also used PC1 F_{ST} scores as input. In cases where multiple change points were detected within close vicinity of one another, caution was taken to delimit the smallest region in each case; this was to correctly identify the minimum unit of inheritance. Within the identified CPD regions, we further inspected the segregation of Iso-Y line alleles responsible for driving differentiation by plotting the AFs of each identified region¹²⁰.

To assess diversity among the Iso-Y lines, π was calculated from the Iso-Y line allele frequencies on a per base pair basis¹²¹. To summarise the among-Iso-Y line variation, per SNP π values were used as input to PCA, calculated using the *prcomp* function.

For functional gene annotation, we extracted the regions of interest from the guppy genome (https://www.ebi.ac.uk/ena/browser/view/GCA_904066995) using *samtools* *faidx* (v1.9)¹⁰² and aligned them to the previous guppy genome assembly (https://www.ebi.ac.uk/ena/browser/view/GCA_000633615.2) using *minimap2* v2.17¹¹⁷ and pulled the uniprot gene IDs from the annotation using *biomaRt* v2.44¹²². GO enrichment and KEGG mapping were performed using *clusterProfiler* v3.18.1¹²³. For KEGG mapping, we used Ensembl's gene dataset for the species as the universe. For GO enrichment, we used the AnnotationHub v2.22.1 to pull the latest available OrgDb (AH86018).

Analysis of the natural population WGS data.

WGS data comprising 26 wild-caught individuals was used to explore the identified Iso-Y regions in natural guppy populations. Linkage disequilibrium (LD) was calculated among polymorphic SNPs for LG1 and LG12. Invariant positions were removed using *bcftools* v1.8¹²⁴, variants were thinned at 5 kb intervals and r^2 values were calculated in *plink* v1.9¹²⁵ bwh.harvard.edu/plink, outputting a square matrix for plotting using *LDheatmap* v1.04¹²⁶.

Shifts in localised heterogeneity have been explained as a potential artefact of chromosomal inversions or long maintained haplotypes. We analysed patterns arising from changes in local ancestry in the natural data using *lostruct* v0.9⁶⁵. Local PCAs were run with three PCs mapped onto three MDS. Mapped eigenvalues > 0.01 were assessed for saturation before defining significant MDS. Significant outlier windows of each MDS were defined by first calculating 3 standard deviations of the mean of the MDS distribution after trimming the 5% tails of each distribution, followed by returning all windows at the extremes of the distribution. To balance loss of power and sensitivity, local PCAs were assessed in both 10 bp and 100 bp windows (Supplementary Fig. 24). We considered the start and end positions of the signature of each MDS as the last region where we found 3 or more adjacent neighbouring windows.

Population genetics statistics were calculated along LG1 and LG12 using *PopGenome* v2.7.5¹²⁷. *Intersex-F_{ST}*, *D_{xy}* and π were calculated in non-overlapping 1 kb windows. *Intersex D_a* was calculated as *D_{xy}* - female π . Outliers were considered if the regions were outside of the upper and lower 95% quantiles of each calculated statistic. GC and repeat content were calculated from the male guppy genome³¹, computed in 1 kb windows.

Analysis of structural variants and coverage. For the medium-coverage WGS data derived from wild-caught individuals we used BreakDancer v1.4.5¹²⁸ and Lumpy-based smooove v0.2.5¹²⁹ using SVtyper v0.7.0¹³⁰. We also applied these two short-read methods to the Iso-Y Pool-seq data, in addition to Manta v1.6.0¹³¹ as the data were high-coverage and PCR-free. SV outputs were filtered depending on the software: BreakDancer SVs were filtered at a confidence score >=99, read group (RG) support >=median RG; manta SVs were filtered at a quality score >=999 and only events where both paired-read and split-read support at values realistic of the overall read depth were retained; for Lumpy/smooove SVs, events that had evidence of both split read and paired end support at realistic read depth values were considered. We excluded SVs <= 10 kb. We also made use of our long-read sequencing data from one Iso-Y line individual (Iso-Y6) using sniffles v1.0.12¹³² and PBSV v2.3.0 (<https://github.com/PacificBiosciences/pbsv>). Any suspected SVs were manually inspected in the Integrated Genomics Viewer (IGV v2.4.8;¹³³).

Coverage was estimated from bam files using the *bamCoverage* option of *deeptools* v3.3.1¹³⁴. The first and last 100 kb of each chromosome were trimmed before estimating coverage with a *binSize* = 50, *smoothLength* = 75, and an *effectiveGenomeSize* of 528,351,853 bp (genome size minus masked and trimmed regions). The ends of chromosomes were trimmed because they often showed high peaks of coverage, thereby distorting the normalised measures across the chromosome. Coverage estimates were normalised using RPGC (reads per genomic context). Bins with normalised coverage >4 (four times the expected median of 1) were filtered. For the natural WGS data, coverage was averaged within populations. Outputs were converted to bed files with window sizes of 1 and 10 kb by taking weighted means.

Analyses of multiple haplotypes on LG1. Genotype and haplotype plots were created using Genotype Plot in R¹³⁵. For the haplotype-based analysis, we polarised the phased haplotypes to Iso-Y9. Breakpoints between the phases were quantified by identifying the location (in bp) where phase0 switched to phase1, and vice versa. Switchpoints were quantified in males and females and a switchpoint was considered to be conserved when the locations (within 50 kb) overlapped in two or more individuals.

Inter-chromosomal linkage was calculated as above for intra-chromosomal linkage calculating *r2* values between LG1 and LG12 using the *--inter-chr* flag in *plink* v1.9, outputting a normal pairwise matrix. Results were plotted in R using custom scripts¹²⁰.

Reporting summary. Further information on research design is available in the Nature Research Reporting Summary linked to this article.

Data availability

The DNA sequencing data generated in this study have been deposited in the European Nucleotide Archive (ENA) under the Study Accession [PRJEB36506](https://www.ebi.ac.uk/ena/record/PRJEB36506) with the following codes: SAMEA6512722-SAMEA6512725 (Pool-seq Iso-Y data); SAMEA8750557-SAMEA8750565 (whole-genome sequencing data for Paria); SAMEA8795870-SAMEA8795872 (long-read pacbio data for Iso-Y6). The DNA sequencing data generated for Upper Marianne individuals have been deposited in the ENA under the Study Accession [PRJEB10680](https://www.ebi.ac.uk/ena/record/PRJEB10680) under the accession codes: SAMEA3649957-SAMEA3649973. The male guppy reference genome can be accessed at the ENA under the Accession [GCA_904066995](https://www.ebi.ac.uk/ena/record/GCA_904066995). The female guppy reference genome can be accessed at the ENA under Accession [GCA_000633615.2](https://www.ebi.ac.uk/ena/record/GCA_000633615.2). Source data are provided with this paper at <https://github.com/josieparis/guppy-colour-polymorphism>; <https://doi.org/10.5281/zenodo.5036659>. Recombination data were provided through personal communication with permission of the authors.

Code availability

All code, scripts and additional data related to analysis are available on GitHub (<https://github.com/josieparis/guppy-colour-polymorphism>; <https://doi.org/10.5281/zenodo.5940510>), (<https://github.com/josieparis/gatk-snp-calling>; <https://doi.org/10.5281/zenodo.5903522>) and (https://github.com/JimWhiting91/genotype_plot; <https://doi.org/10.5281/zenodo.5913504>).

Received: 26 April 2021; Accepted: 16 February 2022;

Published online: 09 March 2022

References

- Bachtrog, D. Y-chromosome evolution: emerging insights into processes of Y-chromosome degeneration. *Nat. Rev. Genet.* **14**, 113–124 (2013).
- Williams, T. M. & Carroll, S. B. Genetic and molecular insights into the development and evolution of sexual dimorphism. *Nat. Rev. Genet.* **10**, 797–804 (2009).
- Connallon, T. & Clark, A. G. Sex linkage, sex-specific selection, and the role of recombination in the evolution of sexually dimorphic gene expression. *Evolution* **64**, 3417–3442 (2010).
- Mckinnon, J. S. & Pierotti, M. E. R. Colour polymorphism and correlated characters: genetic mechanisms and evolution. *Mol. Ecol.* **19**, 5101–5125 (2010).
- Svensson, E. I. Back to basics: using colour polymorphisms to study evolutionary processes. *Mol. Ecol.* **26**, 2204–2211 (2017).
- Orteu, A. & Jiggins, C. D. The genomics of coloration provides insights into adaptive evolution. *Nat. Rev. Genet.* <https://doi.org/10.1038/s41576-020-0234-z> (2020).
- Endler, J. A. Natural Selection on Color Patterns in *Poecilia reticulata*. *Evolution* **34**, 76–91 (1980).
- Houde, A. *Sex, Color, and Mate Choice in Guppies* (Princeton University Press, 1997).
- Brooks, R. & Endler, J. A. Direct and indirect sexual selection and quantitative genetics of male traits in guppies (*Poecilia reticulata*). *Evolution* **55**, 1002–1015 (2001).
- Blows, M. W., Brooks, R. & Kraft, P. G. Exploring complex fitness surfaces: multiple ornamentation and polymorphism in male guppies. *Evolution* **57**, 1622–1630 (2003).
- Hughes, K. A., Rodd, F. H. & Reznick, D. N. Genetic and environmental effects on secondary sex traits in guppies (*Poecilia reticulata*). *J. Evol. Biol.* **18**, 35–45 (2005).
- Houde, A. E. & Endler, J. A. Correlated evolution of female mating preferences and male color patterns in the Guppy *Poecilia reticulata*. *Science* **248**, 1405–1408 (1990).
- Reznick, D. N., Shaw, F. H., Rodd, F. H. & Shaw, R. G. Evaluation of the rate of evolution in natural populations of Guppies (*Poecilia reticulata*). *Science* **275**, 1934–1937 (1997).
- Godin, J.-G. J. & McDonough, H. E. Predator preference for brightly colored males in the guppy: a viability cost for a sexually selected trait. *Behav. Ecol.* **14**, 194–200 (2003).
- Long, K. D. & Houde, A. E. Orange spots as a visual cue for female mate choice in the Guppy (*Poecilia reticulata*). *Ethology* **82**, 316–324 (2010).
- Farr, J. A. Male rarity or novelty, female choice behavior, and sexual selection in the Guppy, *Poecilia Reticulata* Peters (Pisces: Poeciliidae). *Evolution* **31**, 162–168 (1977).
- Hughes, K. A., Du, L., Rodd, F. H. & Reznick, D. N. Familiarity leads to female mate preference for novel males in the guppy, *Poecilia reticulata*. *Anim. Behav.* **58**, 907–916 (1999).
- Hughes, K. A., Houde, A. E., Price, A. C. & Rodd, F. H. Mating advantage for rare males in wild guppy populations. *Nature* **503**, 108–110 (2013).
- Graber, R. E., Senagolage, M., Ross, E., Houde, A. E. & Hughes, K. A. Mate preference for novel phenotypes: a fresh face matters. *Ethology* **121**, 17–25 (2015).
- Daniel, M. J., Koffinas, L. & Hughes, K. A. Mating preference for novel phenotypes can be explained by general neophilia in female Guppies. *Am. Nat.* **196**, 414–428 (2020).
- Olendorf, R. et al. Frequency-dependent survival in natural guppy populations. *Nature* **441**, 633–636 (2006).
- Fraser, B. A., Hughes, K. A., Tosh, D. N. & Rodd, F. H. The role of learning by a predator, *Rivulus hartii*, in the rare-morph survival advantage in guppies. *J. Evol. Biol.* **26**, 2597–2605 (2013).
- Lindholm, A. & Breden, F. Sex chromosomes and sexual selection in poeciliid fishes. *Am. Nat.* **160**, S214–S224 (2002). Suppl. 6.
- Kottler, V. A. & Schartl, M. The colorful sex chromosomes of teleost fish. *Genes* **9**, 233 (2018).
- Winge, Ö. A peculiar mode of inheritance and its cytological explanation. *J. Genet.* **12**, 137–144 (1922).
- Winge, Ö. The location of eighteen genes in *Lebistes reticulatus*. *J. Genet.* **18**, 1–43 (1927).
- Morris, J., Darolti, I., Bloch, N. I., Wright, A. E. & Mank, J. E. Shared and species-specific patterns of nascent Y chromosome evolution in two Guppy species. *Genes* **9**, 238 (2018).
- Tripathi, N. et al. Genetic linkage map of the guppy, *Poecilia reticulata*, and quantitative trait loci analysis of male size and colour variation. *Proc. Biol. Sci.* **276**, 2195–2208 (2009).
- Morris, J., Darolti, I., van der Bijl, W. & Mank, J. E. High-resolution characterization of male ornamentation and re-evaluation of sex linkage in guppies. *Proc. Biol. Sci.* **287**, 20201677 (2020).
- Bergero, R., Gardner, J., Bader, B., Yong, L. & Charlesworth, D. Exaggerated heterochiasmy in a fish with sex-linked male coloration polymorphisms. *Proc. Natl Acad. Sci. USA* **116**, 6924–6931 (2019).
- Fraser, B. A. et al. Improved reference genome uncovers novel sex-linked regions in the Guppy (*Poecilia reticulata*). *Genome Biol. Evol.* **12**, 1789–1805 (2020).
- Kirkpatrick, M. et al. Evolution of the canonical sex chromosomes of the guppy and its relatives. *G3* <https://doi.org/10.1093/g3journal/jkab435> (2021).

33. Whiting, J. R. et al. On the genetic architecture of rapidly adapting and convergent life history traits in guppies. *Heredity*. <https://doi.org/10.1038/s41437-022-00512-6> (2022).
34. Wright, A. E. et al. Convergent recombination suppression suggests role of sexual selection in guppy sex chromosome formation. *Nat. Commun.* **8**, 14251 (2017).
35. Almeida, P. et al. Divergence and remarkable diversity of the Y chromosome in Guppies. *Mol. Biol. Evol.* **38**, 619–633 (2020).
36. Houde, A. E. Sex-linked heritability of a sexually selected character in a natural population of *Poecilia reticulata* (Pisces: Poeciliidae) (guppies). *Heredity* **69**, 229–235 (1992).
37. Hill, W. G. Selection with recurrent backcrossing to develop congenic lines for quantitative trait loci analysis. *Genetics* **148**, 1341–1352 (1998).
38. Kodric-Brown, A. & Johnson, S. C. Ultraviolet reflectance patterns of male guppies enhance their attractiveness to females. *Anim. Behav.* **63**, 391–396 (2002).
39. Valvo, J. J. et al. Using Delaunay triangulation to sample whole-specimen color from digital images. *Ecol. Evol.* **11**, 12468–12484 (2021).
40. Jombart, T. adegenet: a R package for the multivariate analysis of genetic markers. *Bioinformatics* **24**, 1403–1405 (2008).
41. Jombart, T., Devillard, S. & Balloux, F. Discriminant analysis of principal components: a new method for the analysis of genetically structured populations. *BMC Genet.* **11**, 94 (2010).
42. Stankowski, S. et al. Widespread selection and gene flow shape the genomic landscape during a radiation of monkeyflowers. *PLoS Biol.* **17**, e3000391 (2019).
43. Connors, S. A., Trout, J., Ekker, M. & Mullins, M. C. The role of tolloid/mini fin in dorsoventral pattern formation of the zebrafish embryo. *Development* **126**, 3119–3130 (1999).
44. Sha, J. et al. Identification of testis development and spermatogenesis-related genes in human and mouse testes using cDNA arrays. *Mol. Hum. Reprod.* **8**, 511–517 (2002).
45. Lahn, B. T. & Page, D. C. Functional coherence of the human Y chromosome. *Science* **278**, 675–680 (1997).
46. Gautier, A., Le Gac, F. & Lareyre, J.-J. The *gsdf* gene locus harbors evolutionary conserved and clustered genes preferentially expressed in fish previtellogenic oocytes. *Gene* **472**, 7–17 (2011).
47. Liu, Y. et al. Sexually dimorphic expression in developing and adult gonads shows an important role of gonadal soma-derived factor during sex differentiation in olive flounder (*Paralichthys olivaceus*). *Comp. Biochem. Physiol. B Biochem. Mol. Biol.* **210**, 1–8 (2017).
48. Lehmann, A. R., McGibbon, D. & Stefanini, M. Xeroderma pigmentosum. *Orphanet J. Rare Dis.* **6**, 70 (2011).
49. Fogelholm, J. et al. CREBBP and WDR 24 identified as candidate genes for quantitative variation in red-brown plumage colouration in the chicken. *Sci. Rep.* **10**, 1161 (2020).
50. Jang, H. et al. Hematopoietic and neural crest defects in zebrafish *shoc2* mutants: a novel vertebrate model for Noonan-like syndrome. *Hum. Mol. Genet.* **28**, 501–514 (2019).
51. Gu, L.-H. & Coulombe, P. A. Keratin function in skin epithelia: a broadening palette with surprising shades. *Curr. Opin. Cell Biol.* **19**, 13–23 (2007).
52. Schnetkamp, P. P. M. The SLC24 gene family of Na⁺/Ca²⁺-K⁺ exchangers: from sight and smell to memory consolidation and skin pigmentation. *Mol. Asp. Med.* **34**, 455–464 (2013).
53. Shi, Y., Obert, E., Rahman, B., Rohrer, B. & Lobo, G. P. The retinol binding protein receptor 2 (Rbpr2) is required for photoreceptor outer segment morphogenesis and visual function in Zebrafish. *Sci. Rep.* **7**, 16207 (2017).
54. Kmoch, S. et al. Mutations in PNPLA6 are linked to photoreceptor degeneration and various forms of childhood blindness. *Nat. Commun.* **6**, 5614 (2015).
55. Glasauer, S. & Neuhaus, S. Expression of CaBP transcripts in retinal bipolar cells of developing and adult zebrafish. *Matters* 1–4 (2016).
56. Cronin, T. et al. The disruption of the rod-derived cone viability gene leads to photoreceptor dysfunction and susceptibility to oxidative stress. *Cell Death Differ.* **17**, 1199–1210 (2010).
57. Tanaka, T. et al. Tudor domain containing 7 (Tdrd7) is essential for dynamic ribonucleoprotein (RNP) remodeling of chromatoid bodies during spermatogenesis. *Proc. Natl Acad. Sci. USA* **108**, 10579–10584 (2011).
58. Lolicato, F. et al. Potential role of Nanos3 in maintaining the undifferentiated spermatogonia population. *Dev. Biol.* **313**, 725–738 (2008).
59. Roy, A., Lin, Y.-N., Agno, J. E., DeMayo, F. J. & Matzuk, M. M. Absence of tektn 4 causes asthenozoospermia and subfertility in male mice. *FASEB J.* **21**, 1013–1025 (2007).
60. Kottler, V. A., Fadeev, A., Weigel, D. & Dreyer, C. Pigment pattern formation in the guppy, *Poecilia reticulata*, involves the Kita and Csl1ra receptor tyrosine kinases. *Genetics* **194**, 631–646 (2013).
61. Parichy, D. M., Rawls, J. F., Pratt, S. J., Whitfield, T. T. & Johnson, S. L. Zebrafish sparse corresponds to an orthologue of *c-kit* and is required for the morphogenesis of a subpopulation of melanocytes, but is not essential for hematopoiesis or primordial germ cell development. *Development* **126**, 3425–3436 (1999).
62. Braasch, I., Volf, J.-N. & Schartl, M. The evolution of teleost pigmentation and the fish-specific genome duplication. *J. Fish. Biol.* **73**, 1891–1918 (2008).
63. Domyan, E. T. et al. Epistatic and combinatorial effects of pigmentary gene mutations in the domestic pigeon. *Curr. Biol.* **24**, 459–464 (2014).
64. Murisier, F. & Beermann, F. Genetics of pigment cells: lessons from the tyrosinase gene family. *Histol. Histopathol.* **21**, 567–578 (2006).
65. Li, H. & Ralph, P. Local PCA shows how the effect of population structure differs along the genome. *Genetics* **211**, 289–304 (2019).
66. Gutiérrez-Valencia, J., Hughes, P. W., Berdan, E. L. & Slotte, T. The genomic and evolutionary fates of supergenes. *Genome Biol. Evol.* **13**, evab057 (2021).
67. Charlesworth, D. et al. Using GC content to compare recombination patterns on the sex chromosomes and autosomes of the guppy, *Poecilia reticulata*, and its close outgroup species. *Mol. Biol. Evol.* <https://doi.org/10.1093/molbev/msaa187> (2020).
68. Kim, K.-W. et al. A sex-linked supergene controls sperm morphology and swimming speed in a songbird. *Nat. Ecol. Evol.* **1**, 1168–1176 (2017).
69. Jones, P. et al. Frequency of folate-related polymorphisms varies by skin pigmentation. *Am. J. Hum. Biol.* **30**, e23079 (2018).
70. Nanda, I. et al. Sex chromosome polymorphism in guppies. *Chromosoma* **123**, 373–383 (2014).
71. Dor, L. et al. Mapping of the sex determining region on linkage group 12 of Guppy (*Poecilia reticulata*). *G3* **9**, 3867–3875 (2019).
72. Mitchell, P. S., Sandstrom, A. & Vance, R. E. The NLRP1 inflammasome: new mechanistic insights and unresolved mysteries. *Curr. Opin. Immunol.* **60**, 37–45 (2019).
73. Hosseini, S. et al. Genetic mechanism underlying sexual plasticity and its association with colour patterning in zebrafish (*Danio rerio*). *BMC Genomics* **20**, 341 (2019).
74. Lisachov, A. P., Zadesenets, K. S., Rubtsov, N. B. & Borodin, P. M. Sex chromosome synapsis and recombination in male guppies. *Zebrafish* **12**, 174–180 (2015).
75. Lemos, B., Araripe, L. O. & Hartl, D. L. Polymorphic Y chromosomes harbor cryptic variation with manifold functional consequences. *Science* **319**, 91–93 (2008).
76. Jiang, P.-P., Hartl, D. L. & Lemos, B. Y not a dead end: epistatic interactions between Y-linked regulatory polymorphisms and genetic background affect global gene expression in *Drosophila melanogaster*. *Genetics* **186**, 109–118 (2010).
77. Gordon, S. P., López-Sepulcre, A. & Reznick, D. N. Predation-associated differences in sex linkage of wild guppy coloration. *Evolution* **66**, 912–918 (2012).
78. Rodd, F. H. & Reznick, D. N. Variation in the demography of guppy populations: the importance of predation and life histories. *Ecology* **78**, 405–418 (1997).
79. Pettersson, L. B., Ramnarine, I. W., Becher, S. A., Mahabir, R. & Magurran, A. E. Sex ratio dynamics and fluctuating selection pressures in natural populations of the Trinidadian guppy, *Poecilia reticulata*. *Behav. Ecol. Sociobiol.* **55**, 461–468 (2004).
80. McKellar, A. E., Turcotte, M. M. & Hendry, A. P. Environmental factors influencing adult sex ratio in Trinidadian guppies. *Oecologia* **159**, 735–745 (2009).
81. Arendt, J. D., Reznick, D. N. & López-Sepulcre, A. Replicated origin of female-biased adult sex ratio in introduced populations of the trinidadian guppy (*Poecilia reticulata*). *Evolution* **68**, 2343–2356 (2014).
82. Zeng, K., Charlesworth, B. & Hobolth, A. Studying models of balancing selection using phase-type theory. *Genetics* **218**, iyab055 (2021).
83. Kim, K.-W. et al. Genetics and evidence for balancing selection of a sex-linked colour polymorphism in a songbird. *Nat. Commun.* **10**, 1852 (2019).
84. Kirkpatrick, M. & Hall, D. W. Sexual selection and sex linkage. *Evolution* **58**, 683–691 (2004).
85. Kasimatis, K. R., Ralph, P. L. & Phillips, P. C. Limits to genomic divergence under sexually antagonistic selection. *G3 Genes|Genomes|Genet.* **9**, 3813–3824 (2019).
86. Bissegger, M., Laurentino, T. G., Roesti, M. & Berner, D. Widespread intersex differentiation across the stickleback genome—the signature of sexually antagonistic selection? *Mol. Ecol.* **29**, 262–271 (2020).
87. Wilson, C. A. et al. Wild sex in Zebrafish: loss of the natural sex determinant in domesticated strains. *Genetics* **198**, 1291–1308 (2014).
88. Franchini, P. et al. Long-term experimental hybridisation results in the evolution of a new sex chromosome in swordtail fish. *Nat. Commun.* **9**, 1–11 (2018).
89. Haskins, C. P., Haskins, E. F., McLaughlin, J. J. A. & Hewitt, R. E. Polymorphism and population structure in *Lebistes reticulatus*, an ecological study. *Vertebrate Speciat.* **320**, 395 (1961).
90. Charlesworth, D., Bergero, R., Graham, C., Gardner, J. & Yong, L. Locating the sex determining region of linkage group 12 of Guppy (*Poecilia reticulata*). *G3: Genes, Genomes, Genet.* **10**, 3639–3649 (2020).

91. Wright, A. E. et al. On the power to detect rare recombination events. *Proc. Natl Acad. Sci. USA* **116**, 12607–12608 (2019).
92. Whiting, J. R. et al. Drainage-structuring of ancestral variation and a common functional pathway shape limited genomic convergence in natural high- and low-predation guppies. *PLoS Genet.* **17**, e1009566 (2021).
93. Clark, A. G. Natural selection and Y-linked polymorphism. *Genetics* **115**, 569–577 (1987).
94. Hansen, T. F. Why epistasis is important for selection and adaptation. *Evolution* **67**, 3501–3511 (2013).
95. Postma, E., Spyrou, N., Rollins, L. A. & Brooks, R. C. Sex-dependent selection differentially shapes genetic variation on and off the guppy Y chromosome. *Evolution* **65**, 2145–2156 (2011).
96. Rohlf, F. J. The tps series of software. *Hystrix* **26**, 9–12 (2015).
97. Rohlf, F. J. tpsDig2, version 2.30. TpsSeries. Stony Brook: SUNY, Department of Ecology and Evolution (2017).
98. Oksanen, J. et al. vegan: Community Ecology Package. R package version 2.5-5. 2019. (2020).
99. Nicholls, J. A., Double, M. C., Rowell, D. M. & Magrath, R. D. The evolution of cooperative and pair breeding in thornbills *Acanthiza* (Pardalotidae). *J. Avian Biol.* **31**, 165–176 (2000).
100. Martin, M. Cutadapt removes adapter sequences from high-throughput sequencing reads. *EMBnet. J.* **17**, 10–12 (2011).
101. Li, H. Aligning sequence reads, clone sequences and assembly contigs with BWA-MEM. *arXiv* 1303.3997. Preprint at <https://arxiv.org/abs/1303.3997> (2013).
102. Li, H. et al. The Sequence Alignment/Map format and SAMtools. *Bioinformatics* **25**, 2078–2079 (2009).
103. Okonechnikov, K., Conesa, A. & García-Alcalde, F. Qualimap 2: advanced multi-sample quality control for high-throughput sequencing data. *Bioinformatics* **32**, 292–294 (2016).
104. Garrison, E. & Marth, G. Haplotype-based variant detection from short-read sequencing. *arXiv*1207.3907. Preprint at <https://arxiv.org/abs/1207.3907> (2012).
105. Tange, O. Gnu parallel—the command-line power tool. (2018).
106. Tarasov, A., Vilella, A. J., Cuppen, E., Nijman, I. J. & Prins, P. Sambamba: fast processing of NGS alignment formats. *Bioinformatics* **31**, 2032–2034 (2015).
107. Danecek, P. et al. The variant call format and VCFtools. *Bioinformatics* **27**, 2156–2158 (2011).
108. Hivert, V., Leblais, R., Petit, E. J., Gautier, M. & Vitalis, R. Measuring genetic differentiation from Pool-seq data. *Genetics* **210**, 315–330 (2018).
109. Fraser, B. A., Whiting, J. R., Paris, J. R. & Bemis, F. *Guppy genome: V1.0.0 - male guppy genome assembly*. <https://doi.org/10.5281/ZENODO.4020899> (Zenodo, 2020).
110. Willing, E.-M. et al. Genome-wide single nucleotide polymorphisms reveal population history and adaptive divergence in wild guppies. *Mol. Ecol.* **19**, 968–984 (2010).
111. Blondel, L. et al. Evidence for contemporary and historical gene flow between guppy populations in different watersheds, with a test for associations with adaptive traits. *Ecol. Evol.* **9**, 4504–4517 (2019).
112. Paris, J. R., Whiting, J. R. & Fraser, B. A. *josieparis/gatk-snp-calling: gatk-snp-calling*. <https://doi.org/10.5281/zenodo.5903522> (Zenodo, 2022).
113. Browning, B. L., Zhou, Y. & Browning, S. R. A one-penny imputed genome from next-generation reference panels. *Am. J. Hum. Genet.* **103**, 338–348 (2018).
114. Delaneau, O., Zagury, J.-F. & Marchini, J. Improved whole-chromosome phasing for disease and population genetic studies. *Nat. Methods* **10**, 5–6 (2013).
115. Delaneau, O., Howie, B., Cox, A. J., Zagury, J.-F. & Marchini, J. Haplotype estimation using sequencing reads. *Am. J. Hum. Genet.* **93**, 687–696 (2013).
116. Malinsky, M. et al. Whole-genome sequences of Malawi cichlids reveal multiple radiations interconnected by gene flow. *Nat. Ecol. Evol.* **2**, 1940–1955 (2018).
117. Li, H. Minimap2: pairwise alignment for nucleotide sequences. *Bioinformatics* **34**, 3094–3100 (2018).
118. Martin, M. et al. WhatsHap: fast and accurate read-based phasing. *bioRxiv* 085050. Preprint at <https://doi.org/10.1101/085050> (2016).
119. Killick, R. & Eckley, I. changepoint: An R package for changepoint analysis. *J. Stat. Softw.* **58**, 1–19 (2014).
120. Paris, J. R. *josieparis/guppy-colour-polymorphism: Guppy sex-linked polymorphism*. <https://doi.org/10.5281/zenodo.5036659> (Zenodo, 2022).
121. Begun, D. J. et al. Population genomics: whole-genome analysis of polymorphism and divergence in *Drosophila simulans*. *PLoS Biol.* **5**, e310 (2007).
122. Kasprzyk, A. BioMart: driving a paradigm change in biological data management. *Database* **2011**, bar049 (2011).
123. Yu, G., Wang, L.-G., Han, Y. & He, Q.-Y. clusterProfiler: an R Package for comparing biological themes among gene clusters. *OMICS* **16**, 284–287 (2012).
124. Li, H. A statistical framework for SNP calling, mutation discovery, association mapping and population genetic parameter estimation from sequencing data. *Bioinformatics* **27**, 2987–2993 (2011).
125. Purcell, S. et al. PLINK: a tool set for whole-genome association and population-based linkage analyses. *Am. J. Hum. Genet.* **81**, 559–575 (2007).
126. Shin, J.-H., Blay, S., McNeney, B. & Graham, J. & Others. LDheatmap: an R function for graphical display of pairwise linkage disequilibria between single nucleotide polymorphisms. *J. Stat. Softw.* **16**, 1–10 (2006).
127. Pfeifer, B., Wittelsbürger, U., Ramos-Onsins, S. E. & Lercher, M. J. PopGenome: an efficient Swiss army knife for population genomic analyses in R. *Mol. Biol. Evol.* **31**, 1929–1936 (2014).
128. Fan, X., Abbott, T. E., Larson, D. & Chen, K. BreakDancer: identification of genomic structural variation from paired-end read mapping. *Curr. Protoc. Bioinforma.* **45**, 15.6.1–11 (2014).
129. Layer, R. M., Chiang, C., Quinlan, A. R. & Hall, I. M. LUMPY: a probabilistic framework for structural variant discovery. *Genome Biol.* **15**, R84 (2014).
130. Chiang, C. et al. SpeedSeq: ultra-fast personal genome analysis and interpretation. *Nat. Methods* **12**, 966–968 (2015).
131. Chen, X. et al. Manta: rapid detection of structural variants and indels for germline and cancer sequencing applications. *Bioinformatics* **32**, 1220–1222 (2016).
132. Sedlazeck, F. J. et al. Accurate detection of complex structural variations using single-molecule sequencing. *Nat. Methods* **15**, 461–468 (2018).
133. Thorvaldsdóttir, H., Robinson, J. T. & Mesirov, J. P. Integrative Genomics Viewer (IGV): high-performance genomics data visualization and exploration. *Brief. Bioinform.* **14**, 178–192 (2013).
134. Ramirez, F., Dündar, F., Diehl, S., Grüning, B. A. & Manke, T. deepTools: a flexible platform for exploring deep-sequencing data. *Nucleic Acids Res.* **42**, W187–W191 (2014).
135. Whiting, J. R. *JimWhiting91/genotype_plot: Genotype Plot*. <https://doi.org/10.5281/zenodo.5913504> (Zenodo, 2022).

Acknowledgements

We wish to thank Anne Houde for the initial collection of the Iso-Y line fish from the Paria River, and Helen Rodd for the collection of the wild-caught fish from the Paria River. We also wish to thank Jennifer Valvo for assistance in the maintenance of the Iso-Y lines, and Sally Lepzinski for helping to photograph fish. Thanks to Deborah Charlesworth for experimental insight and suggestions. Computational infrastructure support was provided by The University of Exeter's High-Performance Computing (HPC) facility (ISCA). DNA sequencing was performed by the University of Exeter Sequencing Service (ESS). The project was funded by the Natural Environment Research Council (NERC, NE/P013074/1) (J.R.P., B.A.F.), EU Research Council grant (GuppyCon 758382) (B.A.F., J.R.W., M.v.d.V.) and the National Science Foundation of the United States (NSF) ISO-1354775 and DEB-1740466 (M.J.D., K.A.H.).

Author contributions

J.R.P. carried out molecular work for the WGS data, performed genomic and statistical analysis, interpretation, and wrote the manuscript. J.R.W. assisted with analysis and interpretation throughout. M.J.D. conducted the breeding design, performed phenotyping analysis and wrote parts of the manuscript. J.F.O. assisted with analysis, interpretation and figure preparation. P.J.P. performed the molecular lab work for the Pool-seq data. M.v.d.Z. assisted with molecular work and analysis. C.W.W. assisted with analysis of the Pool-seq data. K.A.H. conceived the project, oversaw the breeding experiments, provided analysis and interpretation throughout. B.A.F. conceived and supervised the project, helped with analysis, and co-wrote the manuscript. All authors provided comments on earlier drafts.

Competing interests

The authors declare no competing interests.

Additional information

Supplementary information The online version contains supplementary material available at <https://doi.org/10.1038/s41467-022-28895-4>.

Correspondence and requests for materials should be addressed to Josephine R. Paris.

Peer review information *Nature Communications* thanks Ben Sandkam and the other, anonymous, reviewer(s) for their contribution to the peer review of this work. Peer reviewer reports are available.

Reprints and permission information is available at <http://www.nature.com/reprints>

Publisher's note Springer Nature remains neutral with regard to jurisdictional claims in published maps and institutional affiliations.



Open Access This article is licensed under a Creative Commons Attribution 4.0 International License, which permits use, sharing, adaptation, distribution and reproduction in any medium or format, as long as you give appropriate credit to the original author(s) and the source, provide a link to the Creative Commons license, and indicate if changes were made. The images or other third party material in this article are included in the article's Creative Commons license, unless indicated otherwise in a credit line to the material. If material is not included in the article's Creative Commons license and your intended use is not permitted by statutory regulation or exceeds the permitted use, you will need to obtain permission directly from the copyright holder. To view a copy of this license, visit <http://creativecommons.org/licenses/by/4.0/>.

© Crown 2022